DISPERSION CHARACTERISTICS OF OPTICAL FIBERS WITH LASER ETCHED TAPS IN CLADDING

by

M. Mahaboob Basha

DEPARTMENT OF ELECTRICAL ENGINEERING

INDIAN INSTITUTE OF TECHNOLOGY KANPUR

March, 1996

DISPERSION CHARACTERISTICS OF OPTICAL FIBERS WITH LASER ETCHED TAPS IN CLADDING

A Thesis Submitted

in Partial Fulfillment of the Requirements

for the Degree of

Master of Technology

by

M. Mahaboob Basha

to the

DEPARTMENT OF
ELECTRICAL ENGINEERING
INDIAN INSTITUTE OF TECHNOLOGY, KANPUR

March 1996.

EE-1996-M-BAS-DIS

CERTIFICATE

It is certified that the thesis entitled *"Dispersion Characteristics of Optical Fibers with Laser Etched Taps in Cladding"* by **M. Mahaboob Basha** has been carried out under my supervision and that it has not been submitted elsewhere for the award of a degree.

Anjan K Ghosh 22/3/96

(**Dr. Anjan K. Ghosh**)

Professor

Dept. of Electrical Engg.

IIT Kanpur, INDIA - 208 016

March 1996.

Abstract

Radiative taps can be made in the cladding of optical fibers using the process of laser etching. Study is being carried out on the effect of such taps on the dispersion charcteristics on an equivalent planar dielectric waveguide. A hybrid spectral/mode-matching method has been adopted to calculate the electromagnetic fields guided by such a structure. The advantage of the spectral method is that the Fourier transform automatically enforces the boundary conditions on the taps, and the mode-matching method is straight forward and the solution lends itself to physical interpretation easily. The method thus combines advantages of both the methods. The results show a strong dependance of tap parameters on the dispersion characteristics. This can be utilised in the making of dispersion shifted and dispersion flattened fibers.

Acknowledgements

Iam grateful to Prof. Dr. A. K. Ghosh, my guide, for giving me an oppurtunity to work with him. It has been a extremely invaluable experience that I would cherish.

I would like to thank my friends Ravindra and Balakrishna for their support and affection. I also thank Joshi, Deshpande and Gomati shankar for making my stay here a enjoyable experience.

I thank my parents and brother for their constant support and encouragement.

Basha

Contents

List of Figures

Chapter 1

Introduction

Traditional means of carrying out signal processing in optical communication is to convert the optical signals into electrical signals using photo detectors, and then carry out the processing electronically. However in such a scheme the speed of operation is limited by the speed of operation of the associated electronic circuits, which results in under utilisation of the enormous bandwidth that a optical fiber can offer. Thus, various innovative methods are being put into use to carry out the processing of signals at optical frequencies. A majority of the methods adopt one or the other means to tap out signals from a fiber without causing any major disturbance to the modes propagating inside the fiber. If a series of taps are distributed on an optical fiber, we obtain a fiber optic tapped delayline.

Figure 1.1 shows a typical fiber optic delayline filter. Optical energy is radiated out of the taps made in the cladding of the fiber. Each beam is

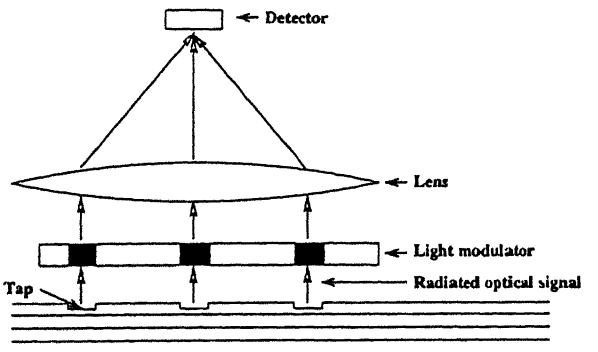

Figure 1.1: Typical fiber optic delayline filter

made to pass through a light modulator, each beam thus passes through materials of different transmittivity. The beams are then collected by a lens and focussed on a detector. Depending on the transmittivities and distance between taps, the detector output changes and thus, the delayline acts as a signal processing filter.

1.1 Methods to tap out optical signals from fiber

Several approaches [2]-[4], [13] to fiber tapping have been proposed such as macro-bending, polishing of the cladding for evanescent couping, slicing and deposition of dielectric mirrors in fiber core, and epoxy attachment of another fiber, local heating to induce divitrification and hence scattering, etc. All the methods mentioned above involve mechanical techniques and thus are not easy, inexpensive and reliable.

A new technique for fabrication of high quality micron-scale fiber-optic taps using ablative chemical etching (LACE) was introduced by Imen et al [2]. This technique involves the use of a CO_2 laser to etch a cut into the cladding of the fiber. The fields propagating in the cladding are refracted and reflected by the facets of the cut thus giving us radiating beams while not significantly affecting the signal propagating in the core.

The set up for the fabrication of taps on optical fibers using the LACE is shown in fig 1.2 . A high power CO_2 laser beam is focussed onto the fiber using a lens and a tap is made by repeated translation of the beam across the fiber. The whole set-up is kept in a reactive gas ambient so as to stop the formation of debris at the edges. As the laser beam has a gaussian profile the resultant cut is gaussian in shape. By controlling the power, pulse time, polarisation and spot size of the beam, the scanning speed and the number of scans a high degree of control is achieved over the depth and width of the cut. With the lateral movement of the fiber along with laser scanning we can obtain shapes other than gaussian, viz ., triangular, rectangular etc.

Radiation properties of such taps have been studied using the traditional

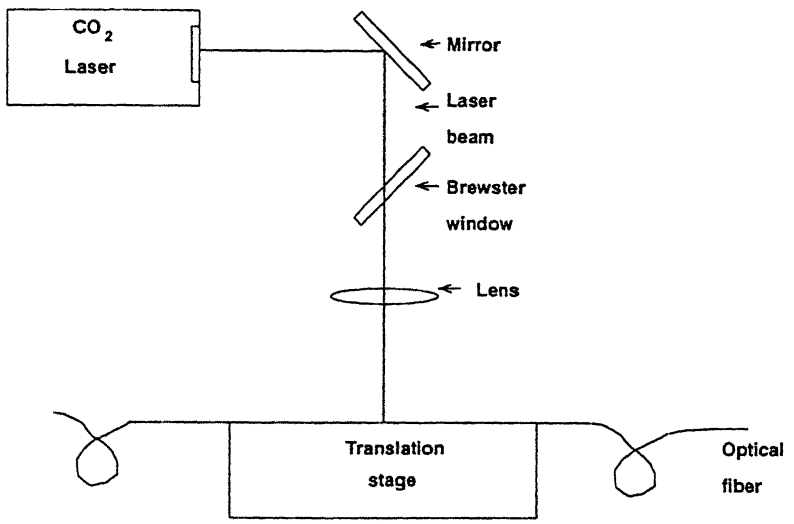

Figure 1.2: The LACE fabrication process

approach representing the cladding fields as rays at various angles by Imen et al [2] . However, it is also important to study the effect of a distribution of LACE taps on the dispersion characteristics of a fiber. A complete analysis of the waveguide dispersion characteristics of a fiber with LACE taps, for various tap geometries may open up applications of tapped fibers in the making of dispersion flattened fibers, dispersion shifted fibers etc.

1.2 Problem overview

In an optical communication system the bandwidth is limited mainly by the spectral width of the source and the dispersion characteristics of the optical fibers. Dispersion in optical fibers can be of various types [17]. There is material dispersion, which occurs because of the fact that the refractive index varies as a nonlinear function of the optical wavelength. As a result various spectral components of a given mode travel at different speeds, depending on the wavelength. Waveguide dispersion, which is dependent on the fiber configuration. Depending on the waveguide configuration the propagation factor is a nonlinear function of the frequency and hence results in different speeds for different optical frequencies. Another form of dispersion

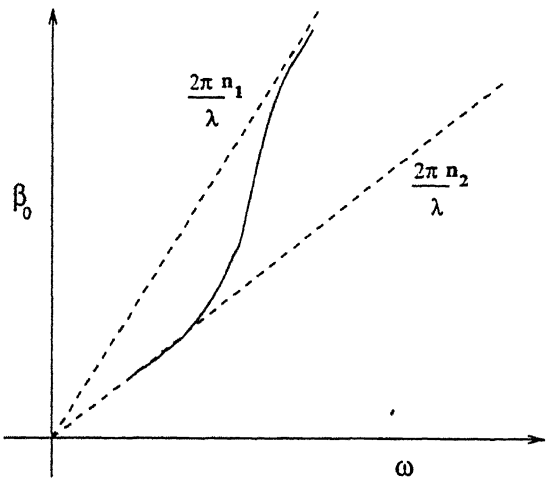

Figure 1.3: Waveguide dispersion characteristics of optical fiber

is the intermodal dispersion, which is a result of different values of group delay for each mode at the same frequency. This mechanism does not affect single-mode operation. In this thesis we investigate the effect of finite number of LACE taps distributed periodically on the waveguide dispersion characteristics of a single mode fiber.

In this thesis analysis has been carried out for the case of a rectangular slab waveguide with taps instead of optical fiber, since it has been shown that the intensity of fundamental TE mode of a rectangular slab is almost similar to LP_{01} mode of a weakly guiding optical fiber for the same core width and refractive indices of core and cladding [17],[14],[10]. For the case of a weakly guiding fiber the difference in the core and cladding refractive indices is very small. In such a fiber the expressions for the field components become simple and the fields thus obtained are similar to the fields in a rectangular slab with the same refractive indices, and with the width of core taken to be equal to the diameter of the core of the fiber.

A hybrid spectral/mode-matching method has been adopted to solve the thesis problem [1],[5]. The method does not employ any approximations and can be applied practically to any dielectric waveguide. Moreover, the solution lends itself to physical interpretations very easily. The method also [illegible] about the mutual coupling between different modes, which

are generated due to the presence of taps. Other methods like FDTD [15],[9] were looked at, but the FDTD method requires at least 12 samples per wavelength which in optical domain gives around 0.1 micron, and also from the fact that the total fields are computed in every iteration. That would result in prohibitively large computation time when dealing with the nature of taps and, distances we were looking at.

The method we use, calculates the electromagnetic fields in different regions of the structure. The solution is then constructed by choosing a suitable combination of these waves so as to satisfy the boundary conditions. The advantage of the spectral method is that the Fourier transform automatically enforces the boundary conditions on the taps. The method thus results in efficient calculation of the electromagnetic fields guided by the structure.

1.3 Overview of the results obtained

From the results of the simulation that have been carried out it has been observed that the propagation constant increases when taps are made in the cladding of the fiber. The propagation constant increases as the number of taps was increased. The propagation constant increases with an increase in tap depth. The increase in tap width does not cause much change in propagation constant. The results show that the propagation constant at a particular wavelength can be changed considerably by varying various tap parameters.

1.4 Organisation of the thesis

In chapter 2 we present the detailed discussion of the spectral/mode matching method. In chapter 3 we discuss the simulation package that has been developed based on the spectral/mode matching method. In chapter 4 we present the results of simulation experiments that have been carried out for various tap parameters using the software that has been developed. In chapter 5 we present the conclusions and scope for further work.

Chapter 2

Spectral/Mode-matching method

In this chapter we discuss the hybrid spectral/mode-matching technique, that has been adopted to solve our thesis problem. The method though rigorous in approach results in efficient calculation of the electromagnetic fields guided by the tapped optical fibers. The strategy adopted is to calculate fields in different regions of the structure. The boundary conditions are then applied to determine the waveguiding properties of the structure [5],[1],[6],[8], [7].

The structure to be analysed as shown in figure 2.1 can be divided into regions in which there is no change in the permittivity in the direction of propagation and, regions in which the permittivity changes along the direction of propagation.

2.1 Maxwell equation's and Wave equation

In the solution of any electromagnetic problem the fundamental relations that must be satisfied are given by Maxwell equations.

$$\nabla \times \vec{E} = -\frac{\partial \vec{B}}{\partial t}, \tag{2.1}$$

$$\nabla \times \vec{H} = \vec{J} + \frac{\partial \vec{D}}{\partial t}, \tag{2.2}$$

$$\nabla \cdot \vec{D} = \rho, \tag{2.3}$$

$$\nabla \cdot \vec{B} = 0, \tag{2.4}$$

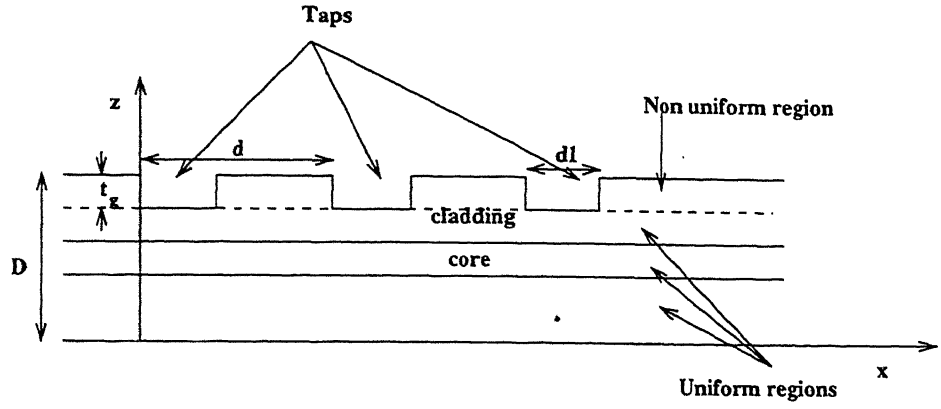

Figure 2.1: Rectangular slab waveguide with rectangular taps in cladding

where, $\vec{E}$ is the electric field vector, $\vec{H}$ is the magnetic field vector, $\vec{D}$ is the electric displacement density vector, $\vec{B}$ is the magnetic flux density vector, $\vec{J}$ is the current density vector and ρ is the volume charge density.

In addition to these relations there are three relations that concern the characteristics of the medium in which the fields exist. These are the constitutive relations.

$$\vec{D} = \epsilon\vec{E}, \tag{2.5}$$

$$\vec{B} = \mu\vec{H}, \tag{2.6}$$

$$\vec{J} = \sigma\vec{E}, \tag{2.7}$$

where, ϵ, μ, σ are the permittivity, permeability, and conductivity of the medium, which is assumed to be homogeneous and isotropic. For a source free region $\vec{J} = 0$ and $\rho = 0$.

Taking curl on both sides of equation (2.1) we have

$$\nabla \times (\nabla \times \vec{E}) = \mu\frac{\partial(\nabla \times \vec{H})}{\partial t} = -\mu\epsilon\frac{\partial^2\vec{E}}{\partial t^2}. \tag{2.8}$$

From the vector identity $\nabla \times (\nabla \times \vec{A}) = \nabla(\nabla \cdot \vec{A}) - \nabla^2\vec{A}$ where, $\vec{A}$ is any vector we can reduce equation (2.8) to

$$\nabla(\nabla \cdot \vec{E}) - \nabla^2\vec{E} = -\mu\epsilon\frac{\partial^2\vec{E}}{\partial t^2}. \tag{2.9}$$

From equation (2.5) and (2.3) for source free region we have

$$\nabla \cdot (\epsilon \vec{E}) = 0. \tag{2.10}$$

Using vector identity $\nabla \cdot (\phi \vec{A}) = \phi \nabla \cdot \vec{A} + \vec{A} \cdot \nabla \phi$ where, $\vec{A}$ is any vector and ϕ is any scalar, equation (2.10) reduces to

$$\epsilon \nabla \cdot \vec{E} + \vec{E} \cdot \nabla \epsilon = 0. \tag{2.11}$$

From equation (2.11) it can be seen that if ϵ is a constant (regions in which there is no change in permittivity in any direction), then $\nabla \cdot \vec{E} = 0$, and equation (2.9) reduces to

$$\nabla^2 \vec{E} - \mu\epsilon \frac{\partial^2 \vec{E}}{\partial t^2} = 0. \tag{2.12}$$

This represents wave equation in uniform regions. For an assumed $exp(-j\omega t)$ time variation of the electric field, equation (2.12) reduces to

$$\nabla^2 \vec{\mathcal{E}} + \omega^2 \mu\epsilon \vec{\mathcal{E}} = 0, \tag{2.13}$$

where $\vec{\mathcal{E}}$ is the electric field phasor, and $\vec{E}(x, y, z, t) = \mathcal{R}e[\mathcal{E}(x, y, z)exp(-j\omega t)]$.

Now let ϵ be a function of direction of propagation x, and let K(x) = $\frac{\epsilon(x)}{\epsilon_0}$ [12],[11] . Then from equation (2.11) we have

$$\nabla \cdot \vec{E} = -\frac{\vec{E} \cdot \nabla K(x)}{K(x)}. \tag{2.14}$$

Substituting equation (2.14) in equation (2.9) we have

$$\nabla[\frac{\vec{E} \cdot \nabla K(x)}{K(x)}] + \nabla^2 \vec{E} - \mu\epsilon_0 K(x) \frac{\partial^2 \vec{E}}{\partial t^2} = 0. \tag{2.15}$$

For an assumed $exp(-j\omega t)$ time variation of the electric field equation (2.15) reduces to

$$\nabla[\frac{\vec{\mathcal{E}} \cdot \nabla K(x)}{K(x)}] + \nabla^2 \vec{\mathcal{E}} + \omega^2 \mu\epsilon_0 K(x) \vec{\mathcal{E}} = 0. \tag{2.16}$$

Equation (2.15) represents the Helmholtz equation for non uniform regions.

2.2 Basic equations

To find out the waveguiding properties of the rectangular slab shown in figure 2.1, Helmholtz equations (2.13) and (2.16) needs to be solved and the type of waves that may appear in every region need to be calculated. The solution is then constructed by choosing a suitable combination of these waves so as to satisfy the boundary conditions. We assume the width of the slab to be infinite in y-direction, and the fields are invariant with respect to the y-coordinate, i.e., $\frac{\partial}{\partial y} = 0$. And hence the fields can be decomposed into TE and TM modes, the Helmholtz equation for the field vectors then reduces to a scalar equation. If the layer with taps, with its width equal to the tap depth were not present then, the characteristic waves in the uniform regions appear in the form

$$\mathcal{E}_i(x,z) = \mathcal{E}_0^{(i)} exp[j(\beta x + k_z z)], \tag{2.17}$$

where, $\mathcal{E}_0^{(i)}$ is a constant, i represents the ith uniform medium, ϵ_i the permittivity of the corresponding medium, β is the propagation constant in x direction, k_z propagation constant in z direction. β and k_z are related by the equation

$$\beta^2 + [k_z^{(i)}]^2 = k_0^2 \epsilon_i, \tag{2.18}$$

where, $k_0 = \frac{2\pi}{\lambda}$ is the plane wave propagation constant in air and λ the free space wavelength. In the absence of absorption and scattering losses, uniform layered structures can support surface waves that propagate along x and decay away from the structure in z direction. Such waves are characterised by real values of β and imaginary values of k_z . However, when a perturbed layer is superimposed on the uniform layered structure, the fields are modified to satisfy the boundary conditions on the taps. Under such conditions, fields in all the uniform regions can be represented as a sum of plane waves, and are of the form,

$$\mathcal{E}_i(x,z) = \sum_{n=-\infty}^{\infty} \mathcal{E}_n^{(i)} exp[j(\beta_n x + k_{zn} z)], \tag{2.19}$$

where, $\mathcal{E}_n^{(i)}$ represents the amplitudes of each partial field. The quantity β_n, which is the propagation constant of the nth partial field is related to the

fundamental propagation constant β_0 by the relation

$$\beta_n = \beta_0 + \frac{2\pi n}{d}, (n = 0, \pm 1, \pm 2, \cdots) \tag{2.20}$$

where, d is the distance between successive taps. Each $\mathcal{E}_i$ now satisfies the wave equation. Hence, $k_{zn}^{(i)} = \pm[k_i^2 - \beta_n^2]^{\frac{1}{2}}$.

Fields in the nonuniform regions should satisfy equation (2.16). Now, for the case of a rectangular slab we have assumed, all the fields can be decomposed into TE and TM modes. For TE modes, only $\mathcal{E}_y, \mathcal{H}_x, \mathcal{H}_z$ are the only nonzero components. Now, since only y-component of the electric field is non-zero and also since the permittivity is a function of x the first term in equation (2.16) reduces to zero. The Helmholtz equation in the perturbed region of the waveguide can then be reduced to the scalar equation for TE modes as

$$\nabla^2 \mathcal{E}_y + f^2(x)\mathcal{E}_y = 0, \tag{2.21}$$

where, $f^2(x) = \omega^2 \mu \epsilon_0 K(x)$. If we assume $\mu = \mu_0$ (non-magnetic regions) then equation (2.21) reduces to

$$f^2(x) = \omega^2 \mu_0 \epsilon_0 K(x), = k_0^2 K(x) \tag{2.22}$$

where, k_0 is the plane wave propagation constant in air. The electric and magnetic field vectors in a TE mode are related by the equations,

$$\vec{\mathcal{E}} = \mathcal{E}_y \vec{u_y} \quad \text{and} \quad \vec{\mathcal{H}} = \frac{-j}{\omega \mu_0}(\nabla \times \vec{\mathcal{E}}) \tag{2.23}$$

Now, $f^2(x)$ can be represented as

$$f^2(x) = k_0^2 \sum_{n=-\infty}^{n=\infty} p_n exp(j\frac{2\pi n}{d}x) \tag{2.24}$$

where $p_n s$ are the fourier transform values for a given K(x) and $\frac{2\pi n}{d}$ represents the spatial frequency harmonics arising from perturbations in the cladding structures. Then we can assume a solution for equation (2.21) of the form

$$\mathcal{E}_y = \sum_{n=-\infty}^{n=\infty} q_n(z) exp(i\beta_n x) \tag{2.25}$$

where β_n is given by the equation (2.20) and $q_n(z)$ is any function of z.

Substituting equations (2.24) and (2.25) into equation (2.21) we have

$$\frac{d^2\mathcal{E}_y}{dx^2} + \frac{d^2\mathcal{E}_y}{dz^2} + f^2(x)\mathcal{E}_y = 0. \tag{2.26}$$

Now,

$$\frac{d^2\mathcal{E}_y}{dx^2} = \sum_{n=-\infty}^{n=\infty} -\beta_n^2 q_n(z) exp(j\beta_n x), \tag{2.27}$$

$$\frac{d^2\mathcal{E}_y}{dz^2} = \sum_{l=-\infty}^{l=\infty} \frac{d^2 q_n(z)}{dz^2} exp(j\beta_l x), \tag{2.28}$$

and

$$f^2(x)\mathcal{E}_y = [k_0^2 \sum_{l=-\infty}^{l=\infty} p_l exp(jlx)][\sum_{n=-\infty}^{n=\infty} q_n(z) exp(j\beta_n x)]. \tag{2.29}$$

Adding equations (2.27) (2.28) and (2.29) we have

$$\sum_{n=-\infty}^{n=\infty} a_n q_n(z) exp(j\beta_n x) + \sum_{l=-\infty}^{l=\infty} b_l exp(j\beta_n x) +$$

$$k_0^2 \sum_{n=-\infty}^{n=\infty} \sum_{l=-\infty}^{l=\infty} C_{n,l} exp(j\beta_n x + j\frac{2\pi l}{d} x) = 0, \tag{2.30}$$

where $a_n = -\beta_n^2$,

$b_l = \frac{d^2 q_l(z)}{dz^2}$

and $C_{n,l} = q_n(z) p_l$.

Now from equation (2.20) we have $\beta_n = \beta_0 + \frac{2\pi n}{d}$, therefore equation (2.30) reduces to

$$\sum_{n=-\infty}^{n=\infty} a_n q_n(z) exp(j\beta_0 x + j\frac{2\pi n}{d} x) + \sum_{l=-\infty}^{l=\infty} b_l exp(j\beta_0 x + j\frac{2\pi l}{d} x) +$$

$$k_0^2 \sum_{n=-\infty}^{n=\infty} \sum_{l=-\infty}^{l=\infty} C_{n,l} exp(j\beta_0 x + j\frac{2\pi(n+l)}{d} x) = 0. \tag{2.31}$$

Equation (2.31) is satisfied if

$$b_l = -[k_0^2 \sum_{n=-\infty}^{n=\infty} C_{n,l-n} - a_l]$$

because, the functions $exp[j(\beta_0 + \frac{2\pi n}{d})x]$ and $exp[j(\beta_0 + \frac{2\pi(n+l)}{d})x]$ are orthogonal to each other. Hence, the sum of coefficients in equation (2.31) can be equated to zero. Thus, for say n = 0 we have

$$\frac{d^2 q_0(z)}{dz^2} = -[k_0^2(\cdots + q_{-3}(z)p_3 + q_{-2}(z)p_2 + q_{-1}(z)p_1 + q_0(z)p_0 + q_1(z)p_{-1} + \cdots) - \beta_0^2 q_0(z)]$$

similarly, for n = 1 we have

$$\frac{d^2q_1(z)}{dz^2} = -[k_0^2(\cdots+q_{-2}(z)p_3+q_{-1}(z)p_2+q_0(z)p_1+q_1(z)p_0+q_2(z)p_{-1}+\cdots)-\beta_1^2q_1(z)]$$

Hence, equation (2.31) reduces to a system of differential equations

$$\frac{d^2\bar{q}(z)}{dz^2} = -\bar{\bar{P}}\bar{q}(z), \tag{2.32}$$

where $P_{nl} = k_0^2 p_{n-l} - \beta_n^2\delta_{nl}$, P_{nl} and δ_{nl} representing elements of matrix $\bar{\bar{P}}$ and kronecker delta respectively. Since, equation (2.32) represents system of differential equations with constant coefficients we may assume the solution of the form

$$\bar{q} = \bar{c}exp(\pm j\alpha z), \tag{2.33}$$

where $\bar{c}$ is a constant vector and α is the propagation constant in z direction. Substituting (2.33) back into equation (2.32) we have

$$\bar{\bar{P}}\bar{c} - \alpha^2\bar{c} = 0. \tag{2.34}$$

From equation (2.34) it can be seen that α_m^2 is an eigenvalue of the matrix $\bar{\bar{P}}$, and c_m represents the eigen vector for the corresponding value of α_m^2. Each eigen vector $\bar{c}_m$ now contains elements c_{mn}, so that every complete solution $\mathcal{E}_y$ in the nonuniform region now contains an infinite set of spatial frequencies, each of which has an amplitude c_{mn}. Hence, for equation (2.32) we have a pair of solutions which can be written

$$\bar{q}_m^{(+)}(z) = \bar{c}_m exp(-j\alpha_m z), \tag{2.35}$$

$$\bar{q}_m^{(-)}(z) = \bar{c}_m exp(j\alpha_m z), \tag{2.36}$$

where $q_m^{(\pm)}(z)$ represent waves that travel along positive and negative z axis respectively.

As can be seen from the discussion above, the order of the matrix $\bar{\bar{P}}$ which appears in the calculation of the fields in non uniform regions is infinite. However, in order to implement the spectral/mode-matching method successfully on computer for the calculation of the fundamental propagation constant β_0 for a rectangular slab with taps, it is necessary to truncate the

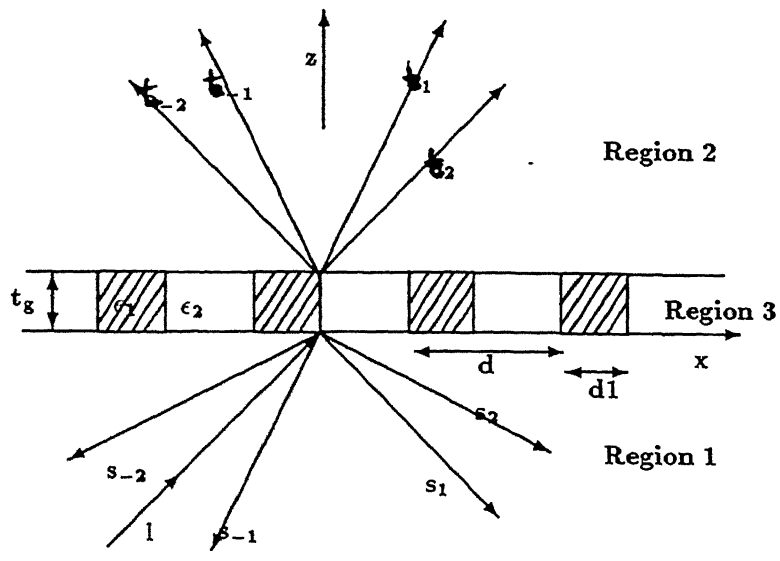

Figure 2.2: Propagation in a single perturbed layer

matrix judiciously. The matrix is of Hill's type and hence, the truncation need not be unduly large for accuracies required by practical considerations. The truncation is found to be valid when we extend the present case to the theory of infinite determinants. We find such a truncation is valid provided [5], [16], [18]

$$(\frac{1}{k_0^2})|k_0^2 p_0 - \beta_n^2 - \alpha_n^2| > \sum_i' |p_i|, \tag{2.37}$$

which must hold for $|n| > N$ where N is a finite positive integer and the prime in the summation indicates that the i = n term is excluded, k_0 is the plane wave propagation constant in free space, and $p_n s$ indicates the value of the Fourier transform for a given profile.

2.3 Field solution for a single non uniform layer

In this section we discuss the problem of calculating the fields supported by a single non uniform layer surrounded by uniform regions as shown in figure 2.2. This solution can then be extended to the actual case of a rectangular slab waveguide with taps in cladding. This is discussed in the next section.

In the figure 2.2 region 1 represents either core or cladding depending on the tap depth, region 2 represents air, and region 3 is the region with taps i.e., the region in which refractive index varies in the direction of propagation. A plane wave of unit amplitude is incident from region 1 and it sets up fields in all the regions. The fields that are setup in various regions can be obtained from the discussion carried out in previous sections this chapter. Using equations (2.25) (2.35) and (2.36) the electric and magnetic field components within the nonuniform layer can be written as

$$\mathcal{E}_3 = \sum_{m=-\infty}^{m=\infty} [g_m^{(+)} exp(j\alpha_m z) + g_m^{(-)} exp(-j\alpha_m z)] \sum_{n=-\infty}^{n=\infty} V_{mn} exp(j\beta_n x), \quad (2.38)$$

$$\mathcal{H}_3 = \sum_{m=-\infty}^{m=\infty} [g_m^{(+)} exp(j\alpha_m z) - g_m^{(-)} exp(-j\alpha_m z)] \sum_{n=-\infty}^{n=\infty} I_{mn} exp(j\beta_n x), \quad (2.39)$$

where, $c_{mn} = V_{mn}$ for TE modes and $c_{mn} = I_{mn}$ for TM modes. If one set is known, other can be calculated using Maxwell equations. $g_m^{(+)}$ and $g_m^{(-)}$ are unknown constants. Using equation (2.19) the fields in region 1, which is a uniform region can then be given by

$$\mathcal{E}_1 = exp(j\beta_0 x + jk_{z0}^{(1)} z) + \sum_{n=-\infty}^{n=\infty} s_n exp((j\beta_n x - jk_{zn}^{(1)} z), \quad (2.40)$$

$$\mathcal{H}_1 = Y_0^{(1)} exp(j\beta_0 x + jk_{z0}^{(1)} z) - \sum_{n=-\infty}^{n=\infty} Y_n^{(1)} s_n exp((j\beta_n x - jk_{zn}^{(1)} z), \quad (2.41)$$

where, s_n are the amplitudes of the scattered waves. Similarly, fields in region 2 can be given by

$$\mathcal{E}_2 = \sum_{n=-\infty}^{n=\infty} t_n exp(j\beta_n x + jk_{zn}^{(2)} z), \quad (2.42)$$

$$\mathcal{H}_2 = \sum_{n=-\infty}^{n=\infty} t_n Y_n^{(2)} exp(j\beta_n x + jk_{zn}^{(2)} z), \quad (2.43)$$

where, $Y_n^{(i)}$ is the characteristic modal admittance given by

$$Y_n^{(i)} = \frac{k_{zn}^{(i)}}{\omega\mu_0} \quad \text{for TE modes and ,} \quad (2.44)$$

$$= \frac{\omega\epsilon_0\epsilon}{k_{zn}^{(i)}} \quad \text{for TM modes} \quad (2.45)$$

and t_n are the amplitudes of radiated waves. Now, applying the boundary conditions at z = 0 for the continuity of electric and magnetic fields and using equations (2.38) (2.39) (2.40) and (2.41) we have

$$\delta_{0n} + s_n = \sum_{m=-\infty}^{m=\infty} V_{mn}[g_m^{(+)} + g_m^{(-)}], \tag{2.46}$$

$$Y_n^{(1)}(\delta_{0n} - s_n) = \sum_{m=-\infty}^{m=\infty} I_{mn}[g_m^{(+)} - g_m^{(-)}], \tag{2.47}$$

similarly, applying boundary conditions to at $z = t_g$ to equations (2.38) (2.39) (2.42) and (2.43) we have

$$\sum_{m=-\infty}^{m=\infty} V_{mn}[exp(j\alpha_m t_g)g_m^{(+)} + exp(-j\alpha_m t_g)g_m^{(-)}] = exp(jk_{zn}^{(2)}t_g)t_n, \tag{2.48}$$

$$\sum_{m=-\infty}^{m=\infty} I_{mn}[exp(j\alpha_m t_g)g_m^{(+)} - exp(-j\alpha_m t_g)g_m^{(-)}] = exp(jk_{zn}^{(2)}t_g)Y_n^{(2)}t_n. \tag{2.49}$$

The equations (2.46) to (2.49) can be written in matrix form, the order of the matrices is equal to the order of matrix $\bar{\bar{P}}$. The matrix $\bar{\bar{P}}$ is truncated using equation (2.37). If N is the order of the truncated matrix then, equation (2.46) can be written in matrix form as

$$\bar{e} + \bar{s} = \bar{V}[\bar{g}^{(+)} + \bar{g}^{(-)}] \tag{2.50}$$

where

$$\bar{e} = \begin{pmatrix} 0 \\ \vdots \\ 1 \\ \vdots \\ 0 \end{pmatrix}, \bar{s} = \begin{pmatrix} s_{\frac{-N}{2}} \\ \vdots \\ s_0 \\ \vdots \\ s_{\frac{N}{2}} \end{pmatrix}, \bar{g}^{(-)} = \begin{pmatrix} g_{\frac{-N}{2}}^{(-)} \\ \vdots \\ g_0 \\ \vdots \\ g_{\frac{N}{2}}^{(-)} \end{pmatrix}, \bar{g}^{(+)} = \begin{pmatrix} g_{\frac{-N}{2}}^{(+)} \\ \vdots \\ g_0 \\ \vdots \\ g_{\frac{N}{2}}^{(+)} \end{pmatrix}$$

and elements of matrix $\bar{\bar{V}} = \{c_{mn}\}$ for TE modes.

Similarly equation (2.47) can be written as

$$\bar{\bar{Y}}_1(\bar{e} - \bar{s}) = \bar{\bar{I}}[\bar{g}^{(+)} - \bar{g}^{(-)}] \tag{2.51}$$

where $\bar{\bar{Y}}_1 = \text{diag}\{Y_n^{(1)}\}$, and $\bar{\bar{I}} = \{c_{mn}\}$ for TM modes.

Equation (2.48) can be written as

$$\bar{\bar{V}}[\overline{\overline{E}}_{xp}^{(+)}\,\bar{g}^{(+)} + \overline{\overline{E}}_{xp}^{(-)}\,\bar{g}^{(-)}] = \overline{\overline{E}}_{kz}\,\bar{t} \tag{2.52}$$

where $\overline{\overline{E}}_{xp}^{(+)} = \text{diag}\{exp(j\alpha_m t_g)\}$, $\overline{\overline{E}}_{xp}^{(-)} = \text{diag}\{exp(-j\alpha_m t_g)\}$ and $\overline{\overline{E}}_{kz} = \text{diag}\{exp(jk_{zn}^{(2)} t_g)\}$. similarly equation (2.49) can be written as

$$\bar{\bar{I}}[\overline{\overline{E}}_{xp}^{(+)}\,\bar{g}^{(+)} - \overline{\overline{E}}_{xp}^{(-)}\,\bar{g}^{(-)}] = \bar{\bar{Y}}_2\overline{\overline{E}}_{kz}\,\bar{t} \tag{2.53}$$

where $\bar{\bar{Y}}_2 = \text{diag}\{Y_n^{(2)}\}$.

Now, premultiplying equation (2.52) with $\bar{\bar{Y}}_2$ and subtracting from equation (2.53) we have

$$(\bar{\bar{I}} - \bar{\bar{Y}}_2\bar{\bar{V}})\overline{\overline{E}}_{xp}^{(+)}\bar{g}^{(+)} - (\bar{\bar{I}} + \bar{\bar{Y}}_2\bar{\bar{V}})\overline{\overline{E}}_{xp}^{(-)}\bar{g}^{(-)} = 0 \tag{2.54}$$

From the above equation we have

$$\bar{g}^{(-)} = (\overline{\overline{E}}_{xp}^{(-)})^{-1}\bar{\bar{R}}_g\overline{\overline{E}}_{xp}^{(+)}\bar{g}^{(+)}$$

where $\bar{\bar{R}}_g = (\bar{\bar{I}} + \bar{\bar{Y}}_2\,\bar{\bar{V}})^{-1}(\bar{\bar{I}} - \bar{\bar{Y}}_2\,\bar{\bar{V}})$. Now, since $\overline{\overline{E}}_{xp}^{(-)}$ is a diagonal matrix its inverse is equal to $\overline{\overline{E}}_{xp}^{(+)}$, hence the above equation reduces to

$$\bar{g}^{(-)} = \overline{\overline{E}}_{xp}^{(+)}\bar{\bar{R}}_g\overline{\overline{E}}_{xp}^{(+)}\bar{g}^{(+)} \tag{2.55}$$

Pre multiplying equation (2.50) with $\bar{\bar{Y}}_1$ and adding to equation (2.51) we have

$$2\bar{\bar{Y}}_1\bar{e} = (\bar{\bar{I}} + \bar{\bar{Y}}_1\bar{\bar{V}})\bar{g}^{(+)} - (\bar{\bar{I}} - \bar{\bar{Y}}_1\bar{\bar{V}})\bar{g}^{(-)}$$

substituting for $\bar{g}^{(-)}$ from equation (2.55) in the above equation we have

$$2\bar{\bar{Y}}_1\bar{e} = [(\bar{\bar{I}} + \bar{\bar{Y}}_1\bar{\bar{V}}) - (\bar{\bar{I}} - \bar{\bar{Y}}_1\bar{\bar{V}})(\overline{\overline{E}}_{xp}^{(+)}\bar{\bar{R}}_g\overline{\overline{E}}_{xp}^{(+)})]\bar{g}^{(+)}$$

Pre multiplying the above equation with $(\bar{\bar{I}} + \bar{\bar{Y}}_1\bar{\bar{V}})^{-1}$ we have

$$\bar{\bar{S}}_g\,\bar{g}^{+} = \bar{\bar{T}}_0\,\bar{e}, \tag{2.56}$$

where

$$\bar{\bar{S}}_g = \bar{\bar{1}} - \bar{\bar{R}}_0\overline{\overline{E}}_{xp}^{(+)}\bar{\bar{R}}_g\overline{\overline{E}}_{xp}^{(+)}, \tag{2.57}$$

$$\bar{\bar{T}}_0 = 2(\bar{\bar{I}} + \bar{\bar{Y}}_1\,\bar{\bar{V}})^{-1}\bar{\bar{Y}}_1, \tag{2.58}$$

$$\bar{\bar{R}}_0 = (\bar{\bar{I}} + \bar{\bar{Y}}_1 \bar{\bar{V}})^{-1}(\bar{\bar{I}} - \bar{\bar{Y}}_1 \bar{\bar{V}}). \tag{2.59}$$

$\bar{\bar{I}}$ is the identity matrix, $\bar{\bar{T}}_0$ and $\bar{\bar{R}}_0$ are transmission and reflection matrices looking into region 1 at z = 0.

In the absence of any incident wave from an exterior region, we have null vector instead of $\bar{e}$ in equation (2.56) which is satisfied only if the determinant of $\bar{\bar{S}}_g$ vanishes. Therefore

$$det(\bar{\bar{S}}_g) = det[\bar{\bar{1}} - \bar{\bar{R}}_0 \bar{\bar{\bar{E}}}_{xp}^{(+)} \bar{\bar{R}}_g \bar{\bar{\bar{E}}}_{xp}^{(+)}] = 0. \tag{2.60}$$

Equation (2.60) represents dispersion relation, solving which yields the unknown value of the propagation constant β_0 . An iterative approach has been followed to solve for β_0 which is described in the next chapter. Similarly by solving for $\bar{g}^{(+)}$ and $\bar{g}^{(-)}$ the fields in the tapped regions can be calculated, and by solving for $\bar{s}$ and $\bar{t}$ the scattered and radiated fields can also be calculated.

2.4 Field solution for rectangular slab with rectangular taps.

The aim of our thesis is to find out the wave guiding properties of the a rectangular slab with taps in cladding as shown in figure 2.1. The problem can be easily solved by making a simple extension to the discussion carried out in the previous section. The rectangular slab with taps in the cladding can be treated as superposition of additional uniform layers below the structure shown in figure 2.2. The problem is further simplified by recognising the fact that superposition of uniform layers below the non-uniform region can be treated as change in admittance matrix at the plane z = 0. And also from the fact that a single non uniform layer can be represented by equivalent transverse network shown in figure 2.3.

In this network, each semi-infinite transmission line (shown by thick line in figure 2.3) represents one of the modes in each region. All the transmission lines are connected to the non uniform region described by the box which represents the matrix $\bar{\bar{S}}_g$. Now the additional uniform layers can be added

below by simply interpolating set of transmission lines of appropriate lengths, as shown in figure 2.4.

In this case at the plane z = $-t_f$ we define reflection coefficient

$$\rho_n = \frac{Y_n^{(1)} - Y_n^{(3)}}{Y_n^{(1)} + Y_n^{(3)}}, \tag{2.61}$$

there by the input admittance at z = 0 is given by

$$Y_n^{in} = Y_n^{(1)} \frac{1 - \rho_n exp(2jk_{zn}^{(1)} t_f)}{1 + \rho_n exp(2jk_{zn}^{(1)} t_f)}. \tag{2.62}$$

Hence the reflection coefficient matrix $\bar{\bar{R}}_0$ as described by equation (2.59) gets modified to

$$\bar{\bar{R}}_0 = (\bar{\bar{I}} + \bar{\bar{Y}}_{in}\bar{\bar{V}})^{-1}(\bar{\bar{I}} - \bar{\bar{Y}}_{in}\bar{\bar{V}}). \tag{2.63}$$

There by the matrix $\bar{\bar{S}}_g$ which is dependent on $\bar{\bar{R}}_0$ also gets modified and hence the propagation constant. Hence to find out the propagation characteristics of a rectangular slab with rectangular taps it is necessary to make the determinant of the modified matrix $\bar{\bar{S}}_g$ zero.

2.5 Field solution for rectangular slab with curved profile taps

In the discussion till the previous section we have concentrated on rectangular taps, however using the spectral/mode-matching method analysis can be done for taps with curved boundaries as well. The approach is to judiciously approximate the curved profiles. Analysis has been carried out for taps having triangular and gausssian shapes as well, as shown in figure 2.5.

The approximation can be done by partitioning the layer with taps into fine layers and approximating each of these by rectangular profile. We thus obtain a configuration as shown in figure 2.6. The analysis of such multiple layered structure can be carried out by straight forward extension of the discussion carried out in the previous sections. It can be seen that the matrix $\bar{\bar{R}}_g$ is the reflection coefficient matrix looking into region 2 at z = t_g in figure 2.2. When a curved profile is approximated by rectangular layers, the matrix $\bar{\bar{R}}_g$ gets modified and hence the propagation constant.

A much simpler, but less accurate [5], way for analysing a curved profile is to average the permittivity for every value of z inside the region with taps. Thus, if the curved boundary that seperates two media that have permittivities ϵ_1 and ϵ_2 is described by a function

$$z = h(x), \quad \text{for } 0 \leq z \leq t_g$$

the averaged permittivity then becomes

$$\epsilon(x) = \epsilon_2 + (\epsilon_2 - \epsilon_1)\frac{h(x)}{t_g}$$

The problem then reduces to that of a layer with uniform thickness but, varying $\epsilon(x)$ and can be solved easily. Since, now the curved profile is approximated just as a change in permittivity in x-direction and hence the problem is similar to that of a rectangular profile, but with a continuous change in the permittivity.

From the discussion that has been carried out in this chapter it is clear that the method can be applied to practically any dielectric waveguide. A simulation package based on the spectral/mode-matching method that has been described in this chapter, has been developed. The package is described in the next chapter.

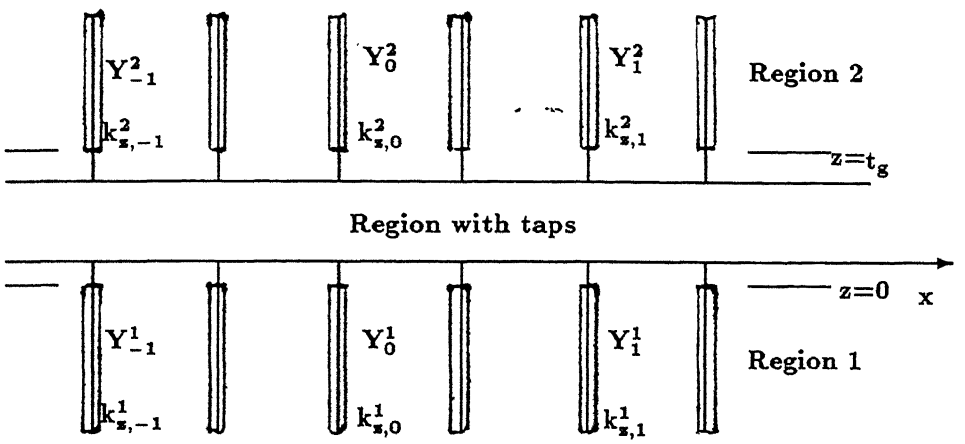

Figure 2.3: Equivalent transverse network for a single nonuniform layer

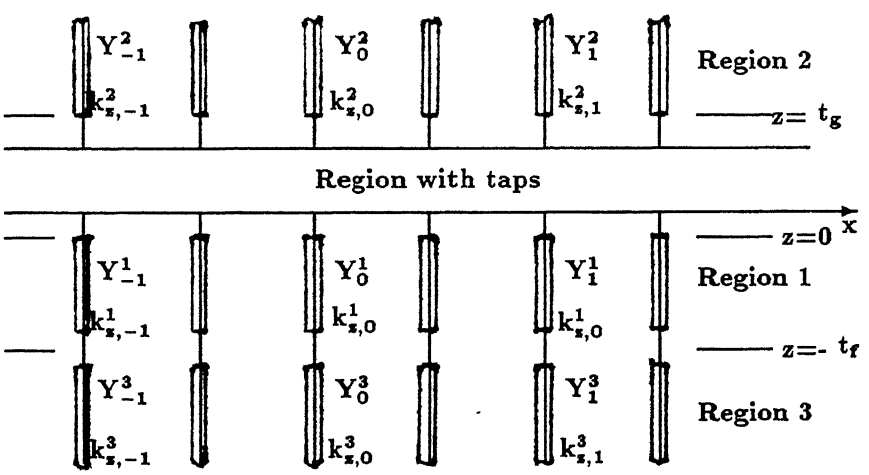

Figure 2.4: Equivalent transverse network for multiple layers

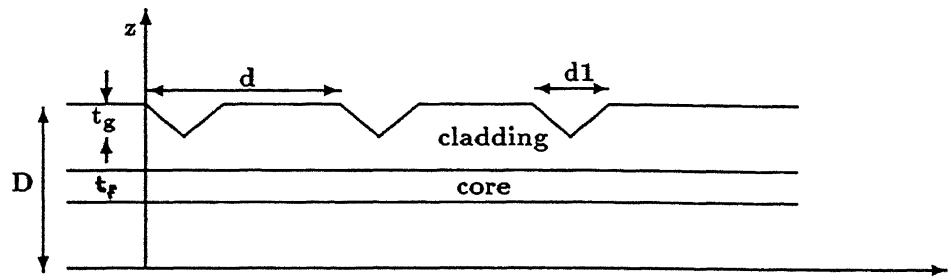

Figure 2.5.1 : Triangular taps

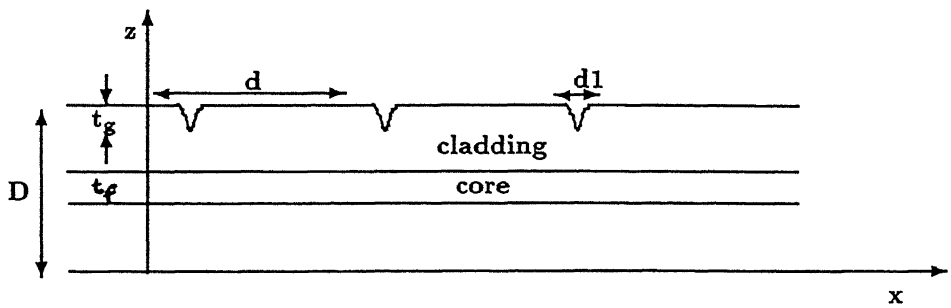

Figure 2.5.2 : Gaussian taps

Figure 2.5: Rectangular slab with curved profile taps

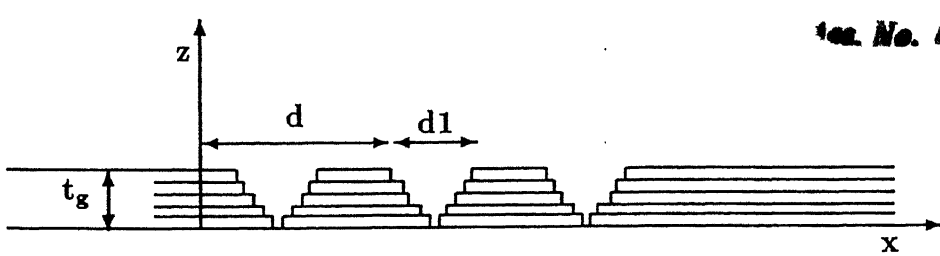

Figure 2.6: Rectangular layer approximation of triangular taps

Chapter 3

Simulation package for spectral/mode-matching method

Based on the spectral/mode-matching technique which was described in the last chapter, we have developed software which gives the propagation characteristics of rectangular slabs with taps in cladding. In this chapter we describe the software that has been developed. We also discuss the validity of the software. To test the validity of the software, propagation characteristics of a rectangular dielectric waveguide were calculated theoretically. The propagation characteristics of the slab were then calculated by the software by making the tap depth equal to zero. The error was found to be less than 1% of the theoretical value at all wavelengths..

3.1 Various issues in software implementation

The application of the spectral/mode-matching technique described in previous involves the solution of the transcendental equation, which involves setting determinant of $\bar{\bar{S}}_g$ given by equation (2.60) to zero. All the parameters entering $\bar{\bar{S}}_g$ are known except for β_0 which is regarded as the unknown variable for any given frequency. In general however, the quantities α_m and c_{mn} (in the region with taps) which are the eigen values and eigen vectors of matrix $\bar{\bar{P}}$ are not known explicitly, so that determination of their values is

part of the computation process for finding β_0.

3.1.1 Truncation of the matrix of infinite order

Truncation of the matrix of infinite order for the calculation of the eigen values of matrix $\bar{\bar{P}}$ forms one of the most important parts of the computation process. The matrix is of Hill's type and hence the matrix need not be of unduly large order. The validity of truncation is checked by making use of the equation (2.37) [16], [18], [5]. To start with, the eigen values are calculated for an assumed order of the matrix, say five. The condition for validity is checked, if the condition is not satisfied the order of matrix is increased by one. In general however the order of the matrices to be dealt with was found to be sufficiently small, typical values being 9 to 15. However, the increase in the order of the matrix increases the accuracy of the result, at the same time results in increase in computational time.

3.1.2 Basic structure of the subroutines to be implemented

A first step in the programming of a computer routine for solving the transcendental equation described by $\bar{\bar{S}}_g$ is to provide routines for calculation of the Fourier transform given the tap shape, width, distance between successive taps number of taps, the refractive indices of cladding and tap filling if any. Since for the tap shapes we were dealing with the Fourier transform can be derived analytically, we used the derived results in calculating the Fourier transform. Once the Fourier transform has been calculated the next step is to find out matrix $\bar{\bar{P}}$ for an assumed value of β_0 , then the eigen values α_m^2 , the eigen vectors $\bar{c}_m$ for an assumed order. The validity of truncation is checked. After the truncation is found to be valid, the matrix $\bar{\bar{S}}_g$ is found, the determinant is calculated. If the determinant is found to be equal to zero, the value of β_0 is that of the actual propagation constant. However, if the determinant is found to be not equal to zero, then the value of β_0 is varied till the determinant of $\bar{\bar{S}}_g$ is found to be equal to zero.

All the routines have been written in "C++" programming language,

except for the routine which calculates the eigen values and eigen vectors of a complex matrix of any order. For calculating the eigen values and eigen vectors of a complex matrix NAG routine has been used, the routine uses similarity transformations to reduce the given matrix into Hessenberg form and then calculates the eigen values and eigen vectors. The flow chart that has been followed is given in figures 3.2 and 3.3.

3.1.3 The main loop

After reading all the input parameters, the program calculates the Fourier transform values for a given set of tap parameters. Since, for the tap shapes we were dealing with the Fourier transform can be derived analytically, we used the derived results in calculating the Fourier transform. The program then enters the main loop (shown in figure 3.2). The range of wavelengths over which we have calculated the propagation characteristics is $0.8\mu m$ to $1.6\mu m(\lambda_{max})$. This range was chosen since, it is the range of interest for optical communication. The program calculates the propagation constant for each wavelength in this range starting from $0.8\mu m$ with an increment of $0.01\mu m(\lambda_{incr})$. The basic idea behind the program is to calculate a suitable value of β_0 which would result in making the determinant of matrix $\bar{\bar{S}}_g$ zero. In order to do this we start with an initial guess for β_0, which was taken to be equal to $1.01\frac{2\pi n_2}{\lambda}$ where, n_2 is the refractive index of cladding, λ being the wavelength of operation. This value was chosen since it is known that for a rectangular slab the value of propagation constant lies between $\frac{2\pi n_2}{\lambda}$ and $\frac{2\pi n_1}{\lambda}$. Using the initial guess and the fourier transform values the elements of matrix $\bar{\bar{P}}$ are found for an assumed order. The eigen values and eigen vectors of the matrix are then calculated using NAG routine. Since the matrix $\bar{\bar{P}}$ is truncated, condition for the validity of the truncation is checked. If the truncation is found to be invalid then, the order of the matrix is increased by 1. If the truncation is found to be valid then the program proceeds further and the elements of matrix $\bar{\bar{S}}_g$ are calculated using the equations derived in the previous chapter. The determinant of matrix $\bar{\bar{S}}_g$ is then calculated. If the determinant is found to be greater than 10^{-6}, the value of determinant

is stored in some temporary memory location, the value of β_0 is increased by 5%, the determinant of matrix $\bar{\bar{S}}_g$ is again calculated following all the steps described above. If the value of determinant turns out to be less than 10^{-6} then the value of β_0 gives the value of the propagation constant. On the other hand if the value determinant is again greater than 10^{-6}, the present value of the determinant is compared with the previous stored value, if the present value of determinant is less than the previous stored value the value of β_0 is further increased otherwise, the value of β_0 is decreased. The method is thus iterative and finally gives the value of β_0, which makes the determinant of matrix $\bar{\bar{S}}_g$ zero (less than 10^{-6}). The value of λ and its corresponding value of β_0 are written in a output file. The value of λ is now incremented by λ_{incr} the value of β_0 is calculated by employing the method described above. This is repeated until the value of λ reaches $1.6\mu m(\lambda_{max})$, after which the program comes out of the main loop. The program thus calculates the value of the propagation constant iteratively.

3.2 The simulation program

In this section we describe the simulation program that has been written in "C++" for the implementation of the spectral/mode-matching method .
Input parameters :

1. The software developed can handle three tap shapes rectangular, triangular, and gaussian.

2. In case of rectangular and triangular (base width of triangle) taps the width of tap (d1) is the input, however in case of gaussian taps, the width of the tap has been taken to be 10 times variance of the gaussian profile (shown in figure 2.5).

3. Number of taps (N).

4. Distance between successive taps (d).

5. Refractive indices of core (n_1), cladding (n_2) and refractive index of tapfilling material if any.

6. Total width of the slab (D).

7. Width of the core (t_f).

8. Depth of taps (t_g).

9. Name of the output files.

Output parameters :

The program stores the output data in two files one of which contains wavelength vs propagation constant data, and the other contains the error in making the determinant of matrix $\bar{\bar{S}}_g$ zero.

3.3 Validity of the simulation program

To check the validity of the program that has been written, we decided to find out the propagation constant at various frequencies by making the tap depth equal to zero in our program , and then compare the values so obtained, with the values of propagation constant obtained by theoretical calculation for a rectangular slab.

3.3.1 Theoretical solution

The electric field of the fundamental TE mode[14] for a planar waveguide is given by

$$E_y(z) = Acos(\kappa z) \text{for} |x| < \frac{d}{2} \tag{3.1}$$

and

$$E_y(z) = Be^{(\gamma z)} \text{for} |x| > \frac{d}{2} \tag{3.2}$$

where d is the core width. A and B are found by equating $Acos(\kappa x)$ and $Be^{(\gamma x)}$ at x= $\frac{d}{2}$. κ and γ are given by

$$\kappa = \frac{2\xi}{d} \tag{3.3}$$

$$\gamma = \frac{2}{d}\sqrt{\frac{V^2}{4} - \xi^2} \tag{3.4}$$

where V is given by

$$V = \frac{2\pi d}{\lambda}\sqrt{n_1^2 - n_2^2} \tag{3.5}$$

where n_1, n_2 are refractive indices of core and cladding respectively and λ the wavelength. ξ is obtained as the solution of the transcendental equation

$$\xi \tan(\xi) = \sqrt{\frac{V^2}{4} - \xi^2} \tag{3.6}$$

This transcendental equation was solved by the bisection method. The lower and upper limits of the propagation constant being $\frac{2\pi n2}{\lambda}$ and $\frac{2\pi n1}{\lambda}$. The propagation constant was obtained for λ varying from $0.8\mu m$ to $1.6\mu m$, for n_1 = 1.4616, n_2 = 1.4571 , the width of core = $3.8\mu m$. For the same parameters the tap depth was made equal to zero in the simulation program and the propagation constant was thus obtained. The figure 3.4 shows the plots of the λ vs β_0 (propagation constant). The plot of λ vs percentage error is shown in figure 3.5 . It can be seen that the error is less than 1% at all the wavelengths.

3.4 Conclusions

In this chapter we have presented the methodology that has been adopted to calculate the effect of taps on the propagation characteristics of the optical fiber. We also showed that the method the sufficiently reliable, and that the method can be applied to any dielectric waveguide, since all the input parameters entering the program can be varied.

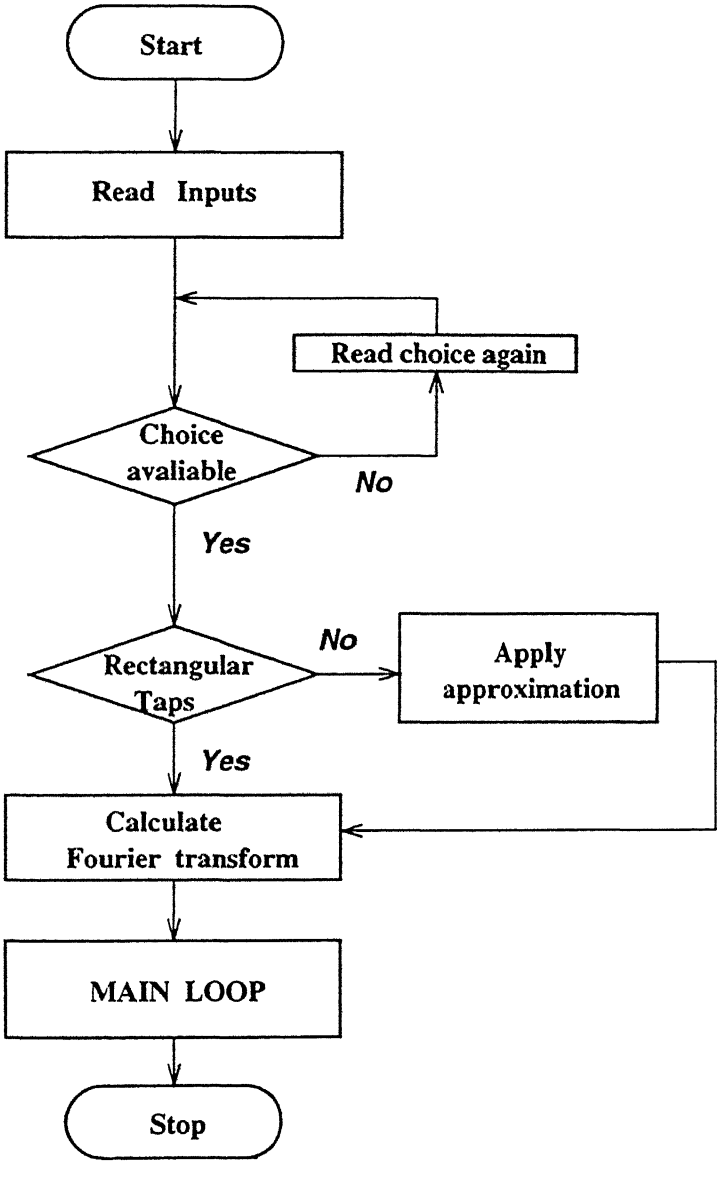

Figure 3.1: Flow chart of Spectral/mode-matching method

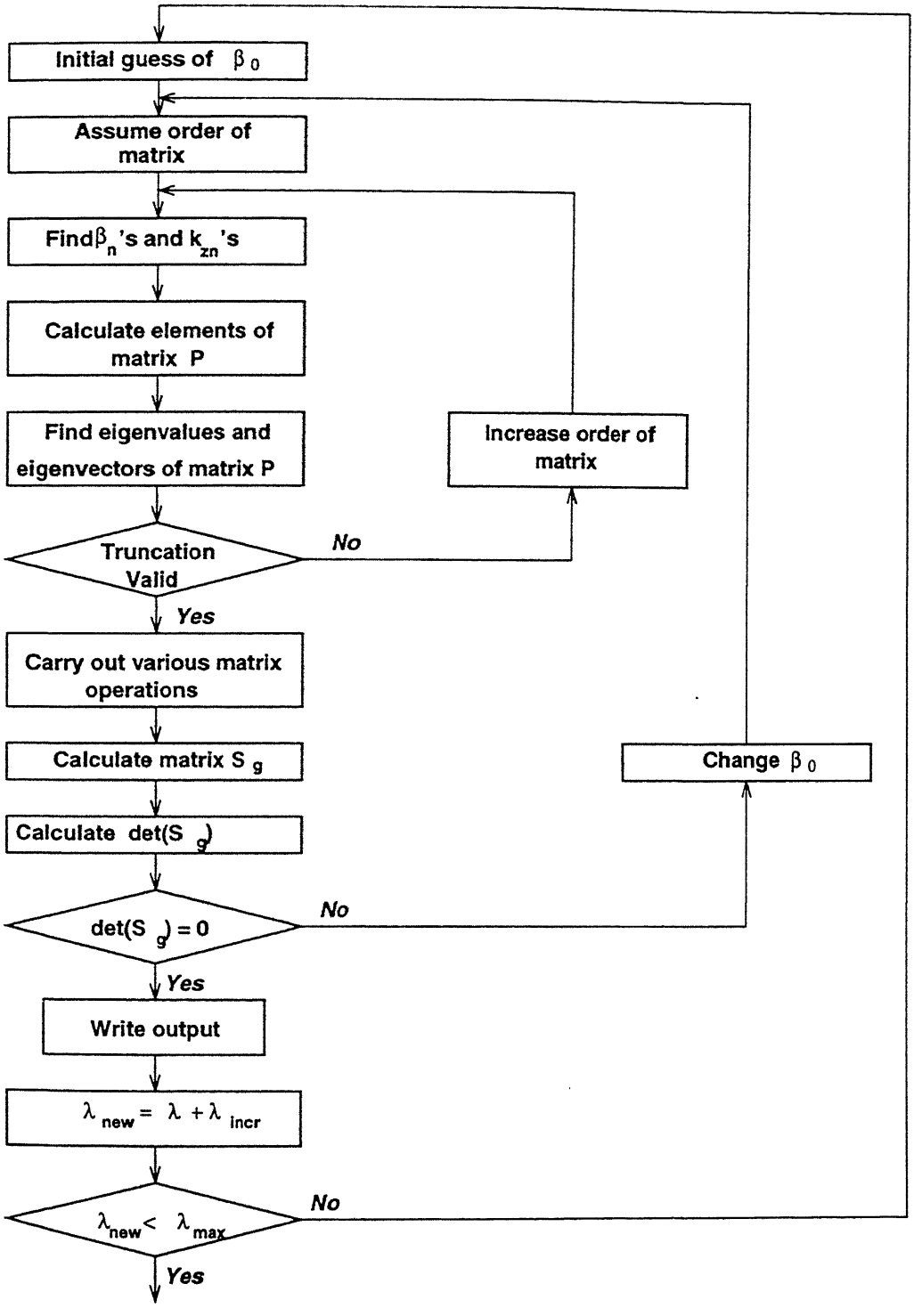

Figure 3.2: Main loop of Spectral/mode-matching method

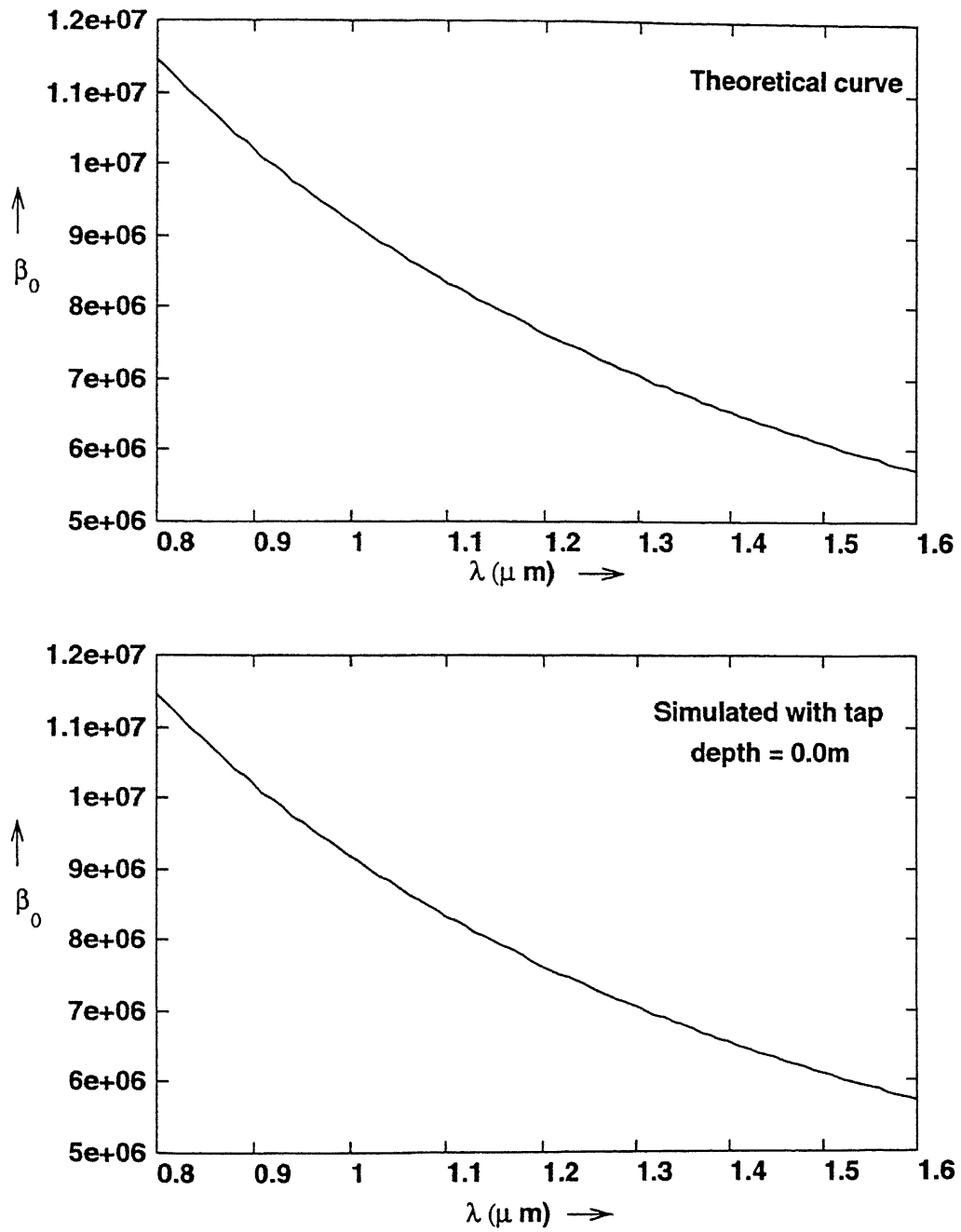

Figure 3.3: Plots showing theoretical and simulated results

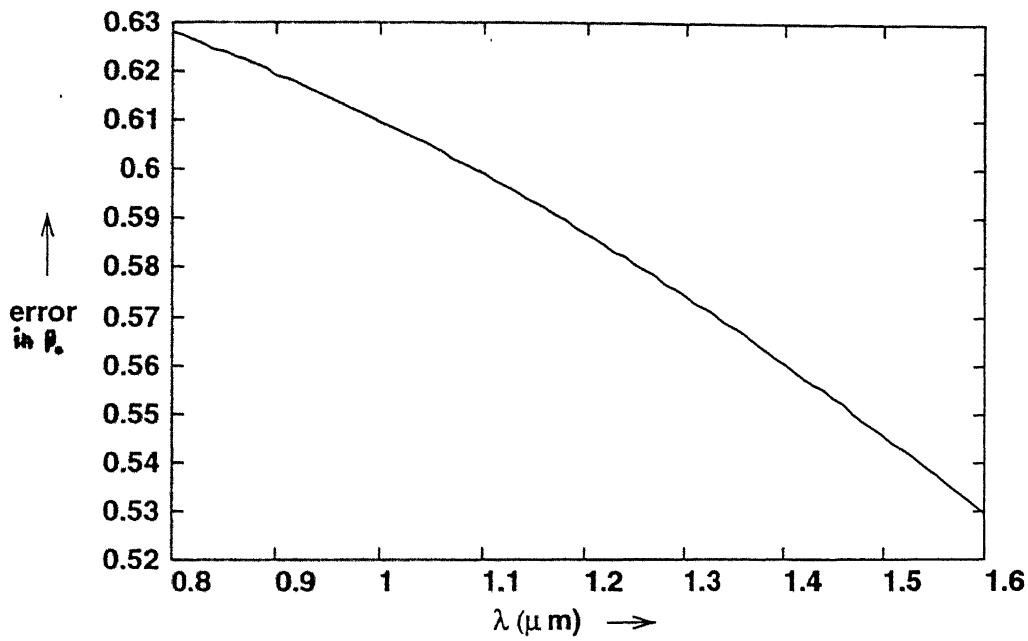

Figure 3.4: Wavelength vs percentage error in propagation constant

Chapter 4

Simulation results

In this chapter we discuss the results that have been obtained from the simulation experiments carried out, based on the spectral/mode-matching approach described in the previous chapters. The results have been obtained for the case of a planar waveguide whose total width and the width of the core were taken to be equal to the diameters of cladding and core respectively of a standard optical fiber. The various input parameters which have been kept constant through out the simulation are

1. Refractive indices of core and the cladding are taken as 1.4616 and 1.4571 respectively.

2. Total width (in z-direction) of the planar waveguide has been kept constant at 125 μm .

3. Width of the core has been taken to be 3.8 μm .

The data is taken from a single mode fiber commercially avaliable [19]. For these parameters the waveguide remains in the single mode over the λ range from $0.8\mu m$ to $1.6\mu m$. The simulation program however, is sufficiently general to handle any values for the above parameters.

The parameters that have been varied are

1. Depth of the taps (t_g), for which we took typical values between 0 to 60.6 μm. For $t_g = 60.6\mu m$ the tap touches the core cladding boundary.

2. Shape of tap, which can be made gaussian, rectangular, and triangular.

Tap parameter	Typical values
Depth	0.0 m to 60.6 μm
Shape	Rectangular, Triangular, Gaussian
Number	10 to 200
Width	20μ m to 200μ m
Distance	100 μ m to 1mm

Figure 4.1: Table showing typical input parameters

3. Number of taps (N), for which typical values were taken between 10 to 200 .

4. The tap width (d1) was varied from $20\mu m$ to $200\mu m$.

5. The distance (d) between taps was varied from $100\mu m$ to 1mm.

4.1 Variation of tap depth

We executed our program several times for different tap parameters. In each case only one parameter was varied keeping all the other parameters constant. Figure 4.1 shows the table of typical values for all the parameters. For each variation we calculated wavelength (λ) vs propagation constant (β_0). The graphs have been plotted with wavelength (λ) on the x-axis and propagation constant (β_0) on the y-axis. Range for wavelength was selected to be $0.8\mu m$ to $1.6\mu m$, since it is the range for optical communication systems.

In this section we present the results that have been obtained by varying the tap depth keeping all other parameters constant. Number of taps was taken to, be equal to 10. Tap width was taken to be equal to $20\mu m$, in case of gaussian taps the width of tap was taken to be equal to be 10 times of the variance. The Distance between successive taps was kept constant at 1mm. The results of the tap depth variation are shown in figures 4.2 and 4.3. The figures show the variation of tap depth for the case of triangular taps. From

the figures 4.2 and 4.3, it can be seen that the propagation constant increases as the tap depth is increased. This can be explained, since an increase in tap depth results in increased radiation from the taps, and hence an increase in tap depth affects the signal propagating inside the fiber However, the effect is more profound at low wavelengths. The propagation constant does not show variations above 5% with respect to the no tap case in the range $1.3\mu m$ to $1.6\mu m$, which is range of interest for optical communication. Hence, it can be concluded that the for small number of taps (10) and tap depths below $40\mu m$, the the increase in propagation constant with the increase in tap depth is below 5%.

4.2 Variation of tap shape

In this section we present the results of variation in the shape of the tap keeping all the parameters except the tap shape constant. The results are shown in figure 4.4. From the figure 4.4 it can be concluded that the variation in tap shape does not affect the propagation characteristics significantly. It can also be seen from the figure 4.4, that the triangular and gaussian taps have similar effect on the propagation characteristics, and hence it can be concluded that the gaussian tap can be approximated to a triangular tap for analysis. It can also be supported by the fact that the spatial frequency spectrum due to the triangular and gaussian taps is similar as shown in figure 4.13.

4.3 Variation of number of taps

In this section we present the results that have been obtained by varying the number of taps keeping all the other parameters constant. The tap width was kept constant at $20\mu m$, the distance between taps was kept constant at 1mm, the tap depth was kept constant at $30\mu m$. From figure 4.5 it can be seen that the propagation constant increases as the number of taps is increased, however again the effect is more profound at low wavelengths. The propagation constant increases for larger wavelengths $1.3\mu m$ to $1.6\mu m$

as the number of taps is increased beyond 100. This can be explained from the fact that as the number of taps is increased the amount of optical energy that is radiated out of the taps also increases, and hence the number of taps have a profound effect on the propagation characteristics of the fiber. Figures 4.6 and 4.7 show the results of variation of number of taps in case of rectangular taps with tap depth equal to $50\mu m$, distance between taps equal to 1mm and width of taps equal to $20\mu m$. As can be seen from the results the increase in the tap depth from $30\mu m$ to $50\mu m$ has more effect on the propagation constant even the range $1.3\mu m$ to $1.6\mu m$. This is supported by the fact that increase in number of taps results higher amplitudes of the spatial frequencies and the increase in tap depth results in more radiation. The spatial frequency spectrum showing the increase in amplitude with the increase in number of taps is shown in figure 4.8.

4.4 Variation of tap width

In this section we present the results that have been obtained by varying the tap width keeping all other parameters constant. The number of taps was kept constant at 10, the distance between taps was kept constant at 1mm and the tap depth was $30\mu m$. From the figures 4.9, 4.10 and 4.11 it can be seen that that the propagation characteristics are not affected by the variation in the tap width in case of rectangular taps however, in case of triangular and gaussian taps the change in tap width does affect the propagation characteristics. This can be explained from the fact that in case of triangular taps a change in tap width keeping the tap depth constant effectively means the change in the angle of the facets of the tap and hence the amount of radiated energy also varies. In case of rectangular taps however, the change in tap width does not effect the angle at which the propagating mode strikes he facets of the taps. Since we were dealing with tap widths much larger ıan the wavelength, the change in the width of a rectangular tap does not ɔw a large effect on the propagation characteristics. In case of gaussian ⁻ a change in tap width means a change in the shape itself, and hence the ⁻gation characteristics are effected by the change in tap width in case

of gaussian taps. However, even in case of triangular and gaussian taps the wavelength range $1.3\mu m$ to $1.6\mu m$ remains unaffected.

4.5 Variation of distance between taps

In this section we present results that have been obtained by varying the distance between taps keeping all other parameters constant. The number of taps was kept constant at 10, the tap width was kept constant at $50\mu m$ and the tap depth was kept constant at $50\mu m$. From the figure 4.12 it can be seen that the propagation characteristics are not effected by the variation in distance between taps. This can again be explained from the fact that the all the distances involved are large compared to the wavelengths.

4.6 Conclusions

It can be concluded from the results of the simulation experiments, that the tap depth and the number of taps have a profound effect on the propagation characteristics of the optical fiber, where as the tap width and the distance between taps do not effect the propagation characteristics of the optical fiber. This fact can be put to use in the making of fiber optic delayline since, in a fiber optic delayline the distances involved are in the range of hundreds of microns and the delayline should not effect the signal propagating inside the fiber. On the other hand the tap depth and the number of taps, which have a profound effect on the propagation characteristics can be used in the making of dispersion less and dispersion flattened fibers.

From the results so obtained, the waveguide dispersion at any desired frequency can be calculated by making use of the formula [11].

$$D_w = -(\frac{n_1 - n_2}{\lambda c}) V \frac{d^2(Vb)}{dV^2}$$

where, λ is the wavelength of operation, c is the velocity of light in free space, n_1 and n_2 are refractive indices of core and cladding respectively, V is the normalised frequency given by

$$V = \frac{2\pi a}{\lambda}\sqrt{n_1^2 - n_2^2}$$

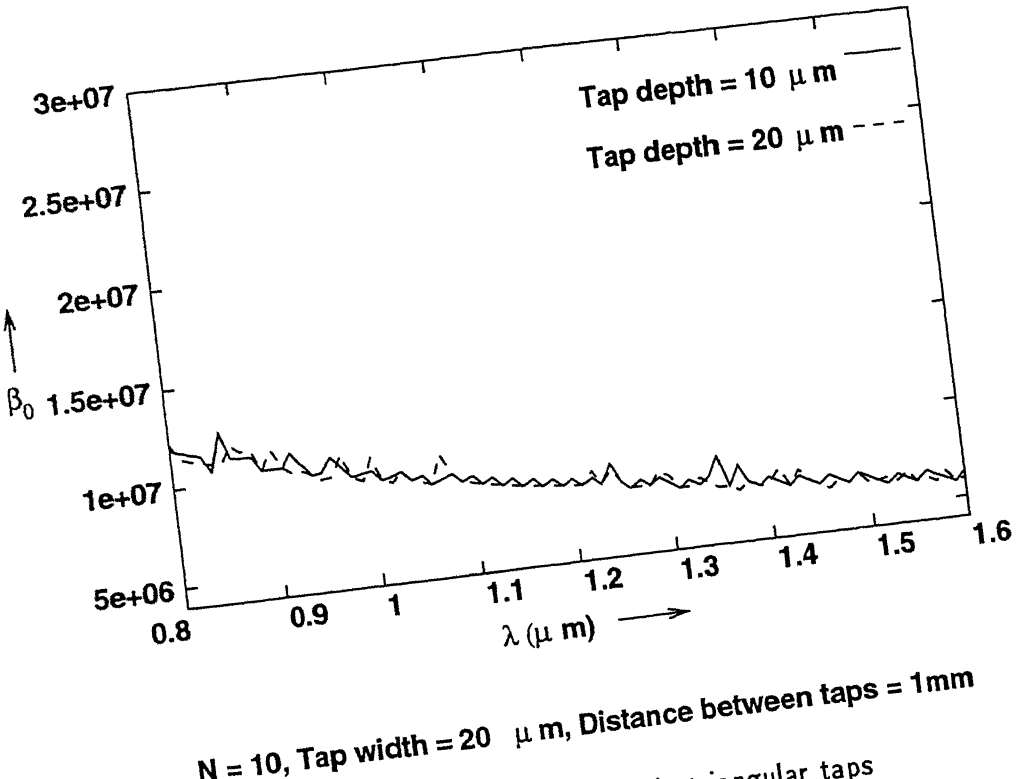

Figure 4.2: Tap depth variation in triangular taps

b is the normalised propagation constant given by

$$b = \frac{(\frac{\beta}{k_0})^2 - n_2^2}{n_1^2 - n_2^2}$$

where k_0 is the free space propagation constant and β is the propagation constant.

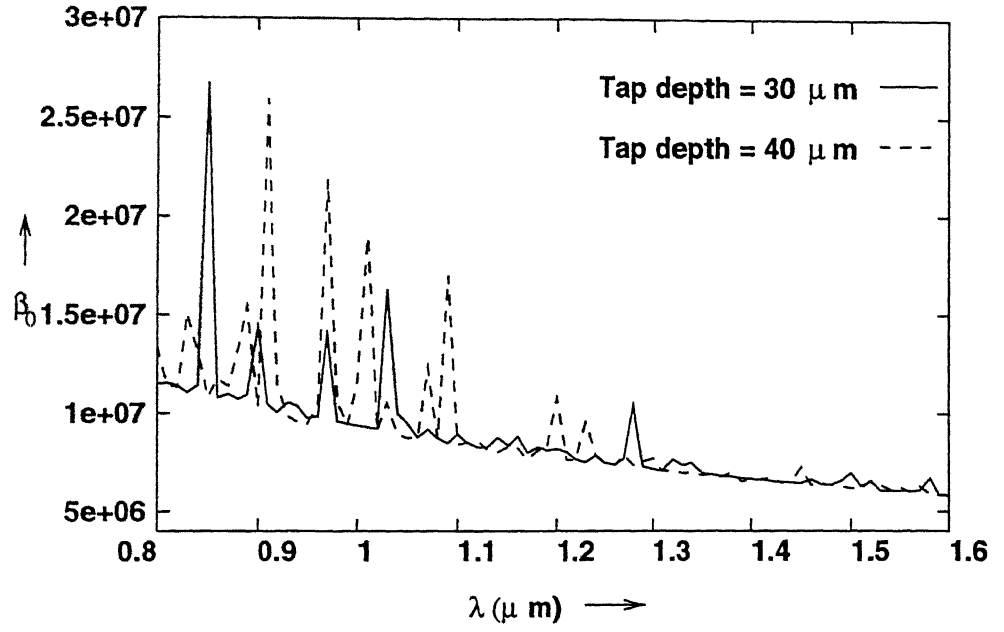

N = 10, Tap width = 20 μ m, Distance between taps = 1mm

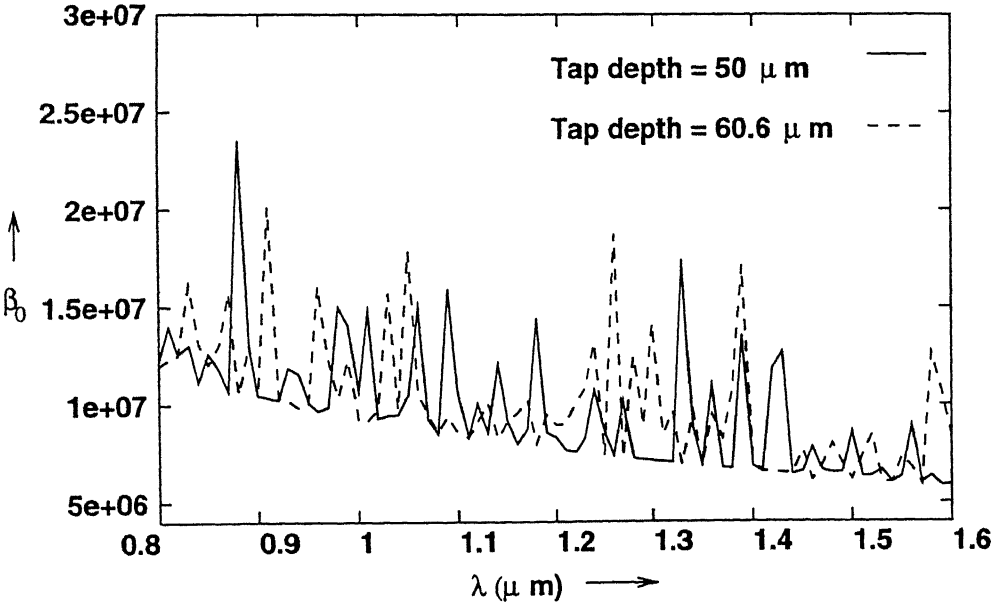

N = 10, Tap width = 20 μ m, Distance between taps = 1mm

Figure 4.3: Tap depth variation in triangular taps

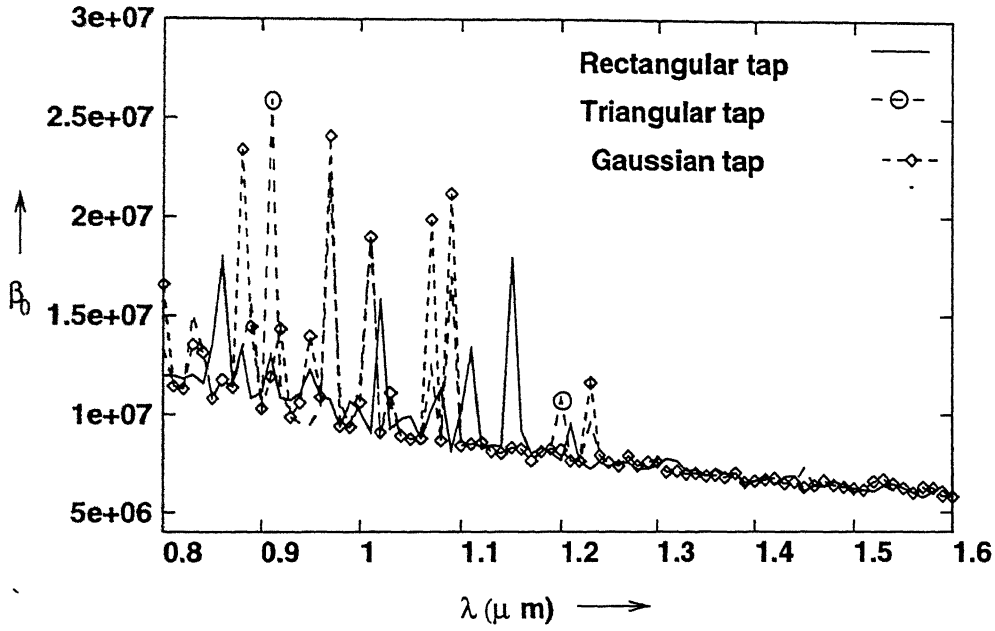

N = 10, Tap width = 20 μ m, Tap depth = 40 μ m, Distance between taps = 1mm

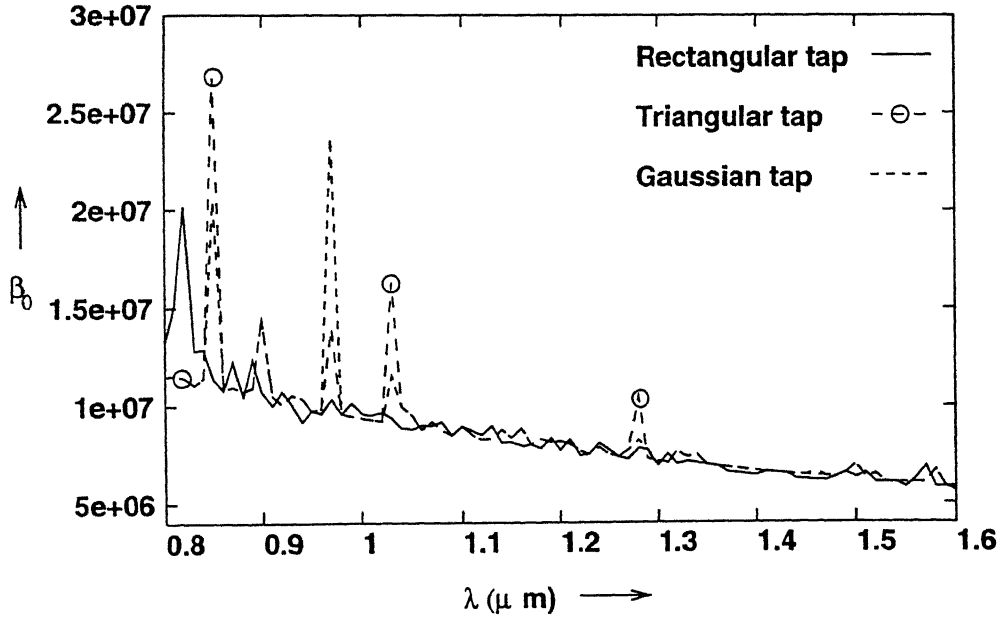

N = 10, Tap width = 20 μ m, Tap depth = 30 μ m, Distance between taps = 1mm

Figure 4.4: Comparison of tap depth variation and tap shape

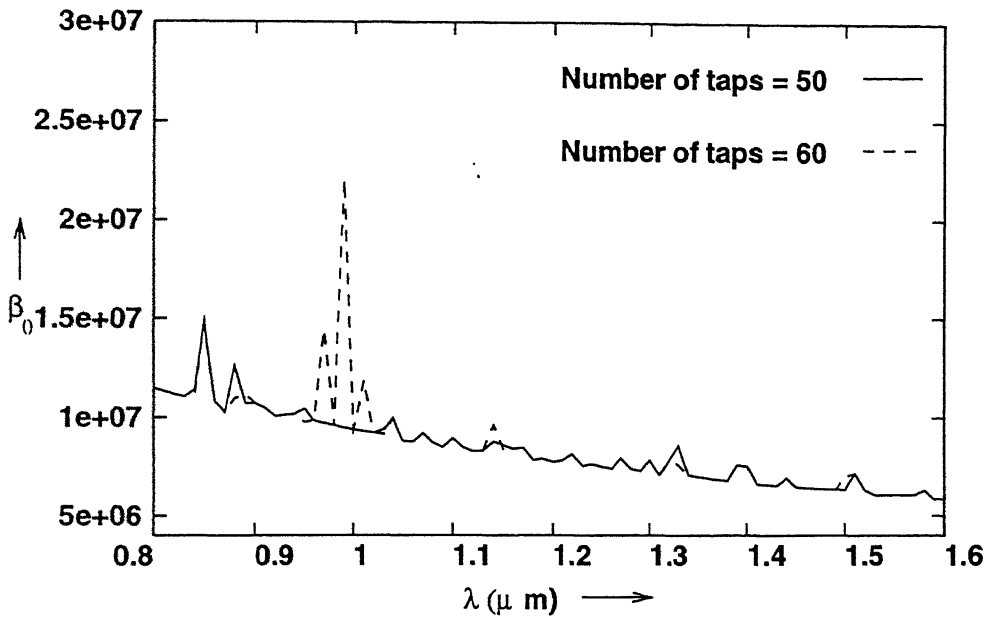

Tap depth = 30 μ m, Tap width = 20 μ m, Distance between taps = 1mm

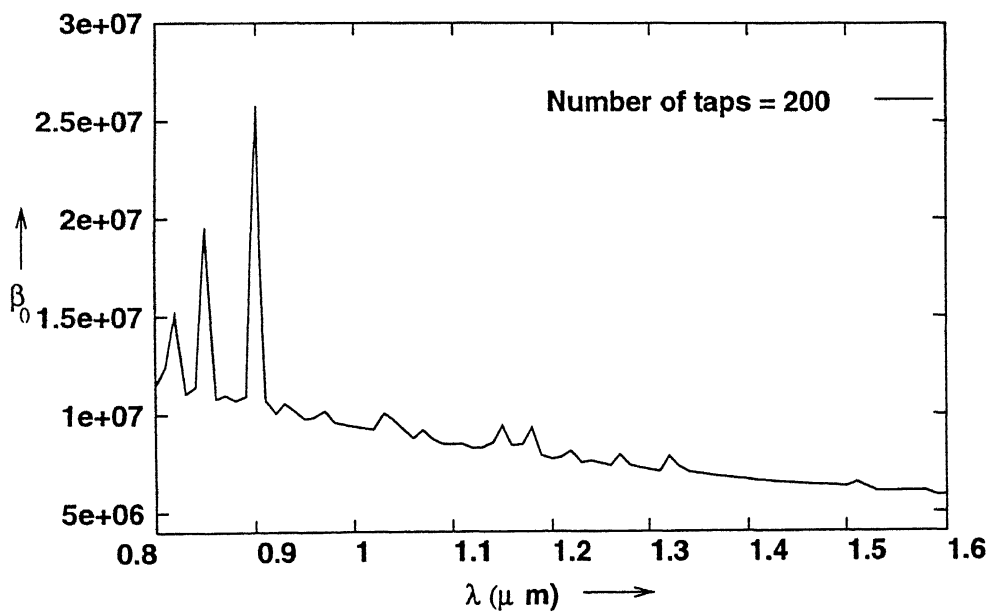

Tap depth = 30 μ m, Tap width = 20 μ m, Distance between taps = 1mm

Figure 4.5: Variation of number of taps in rectangular taps

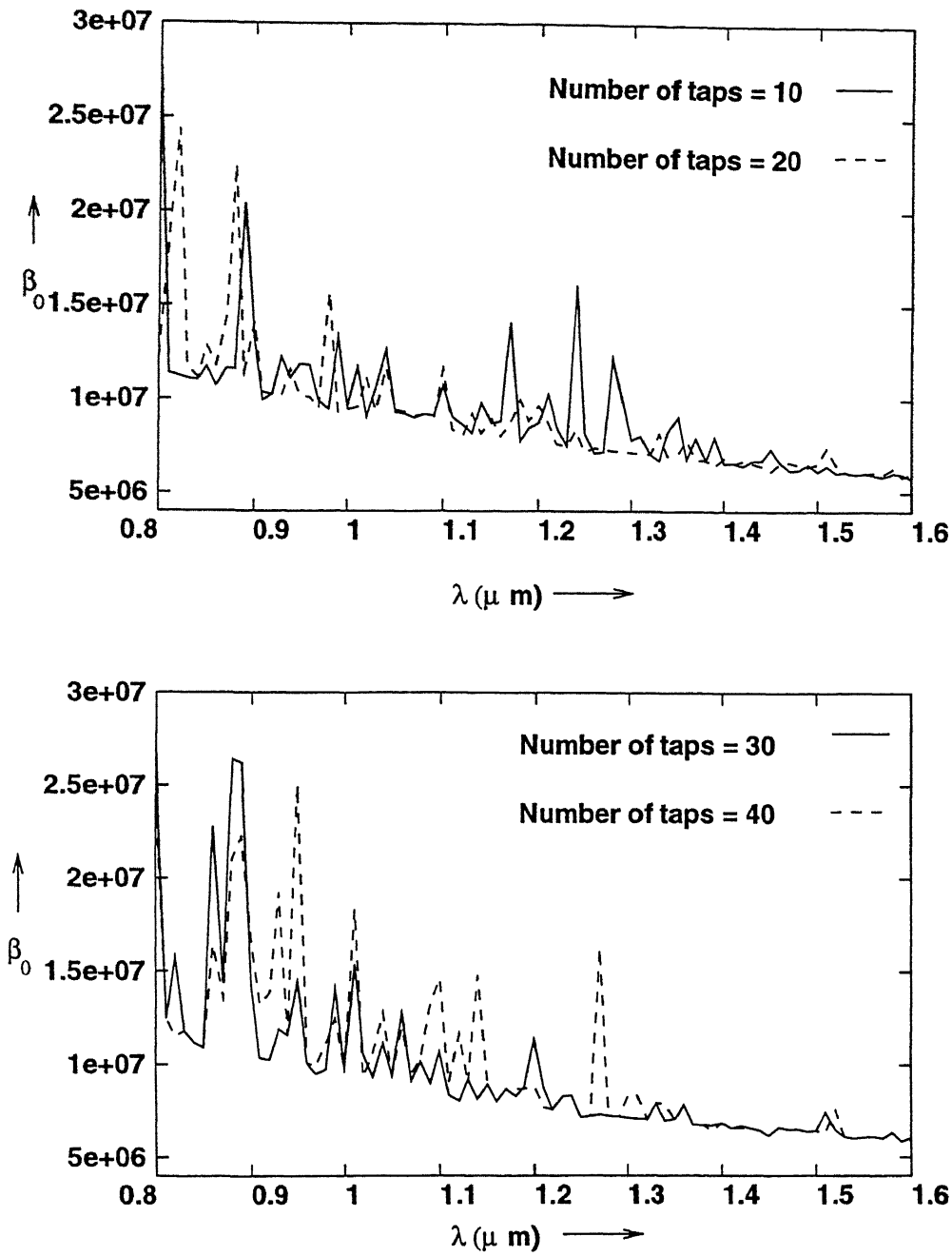

Tap depth = 50 μ m, Tap width = 20 μ m,Distance between taps = 1mm

Figure 4.6: Variation of number of taps in rectangular taps

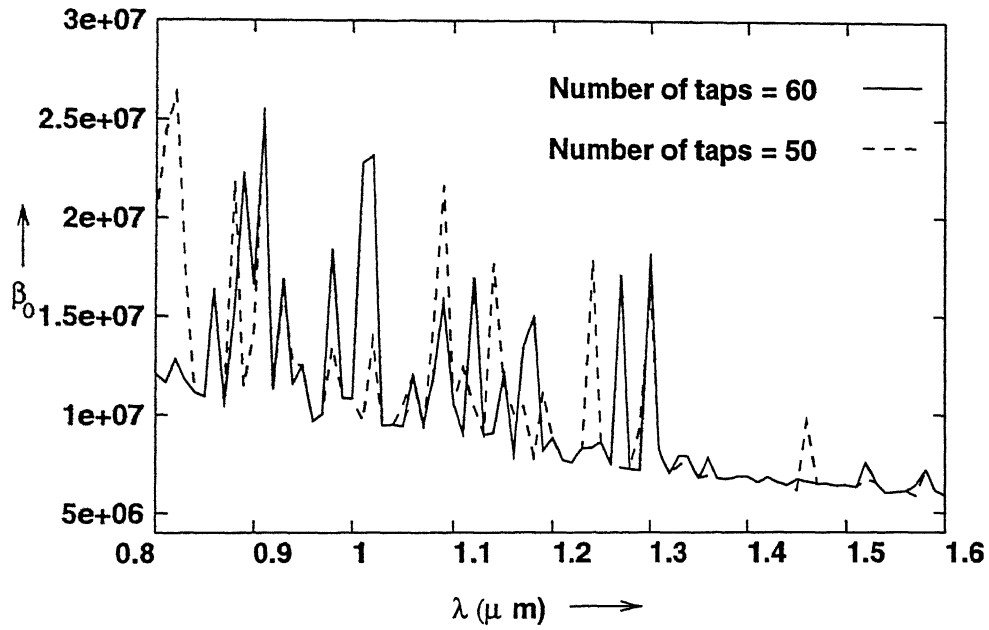

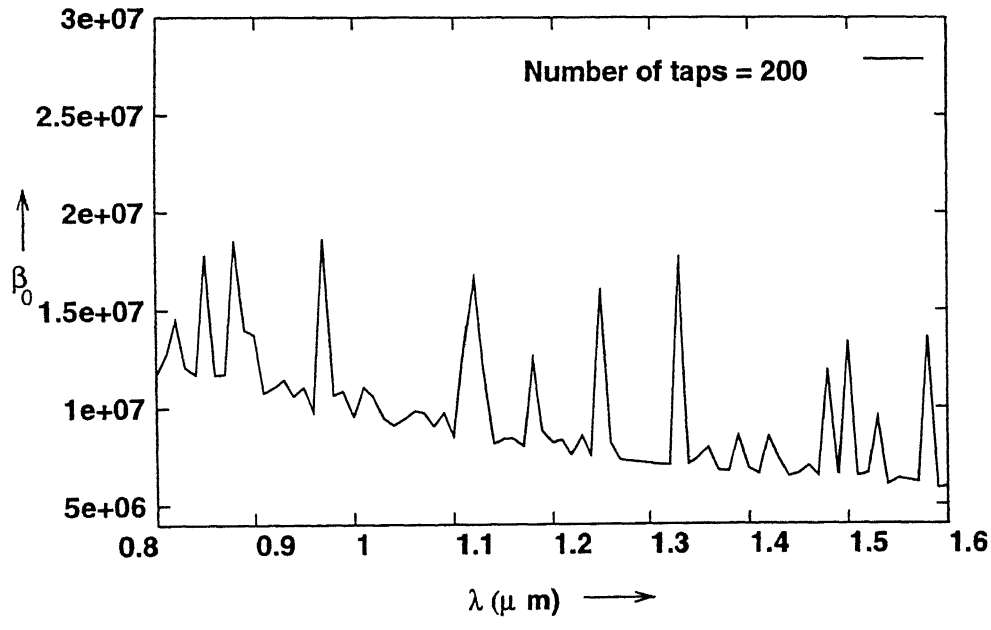

Figure 4.7: Variation of number of taps in rectangular taps

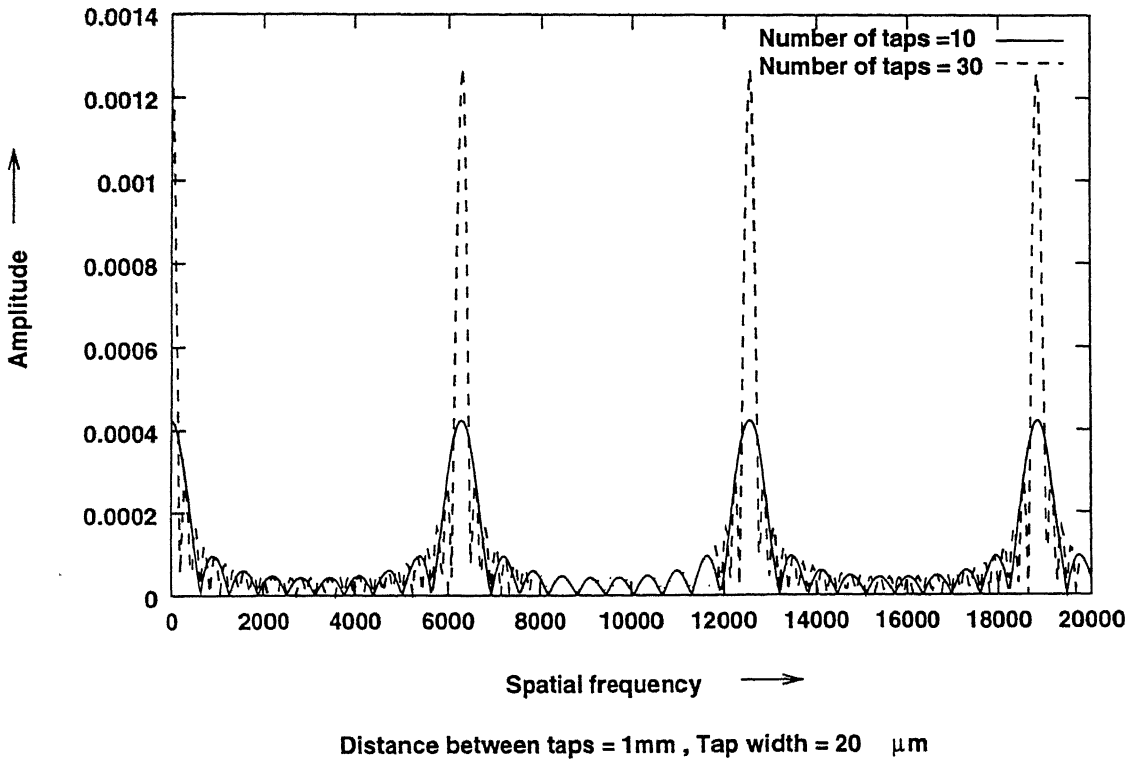

Figure 4.8: Spatial frequency spectrum for variation in number of taps

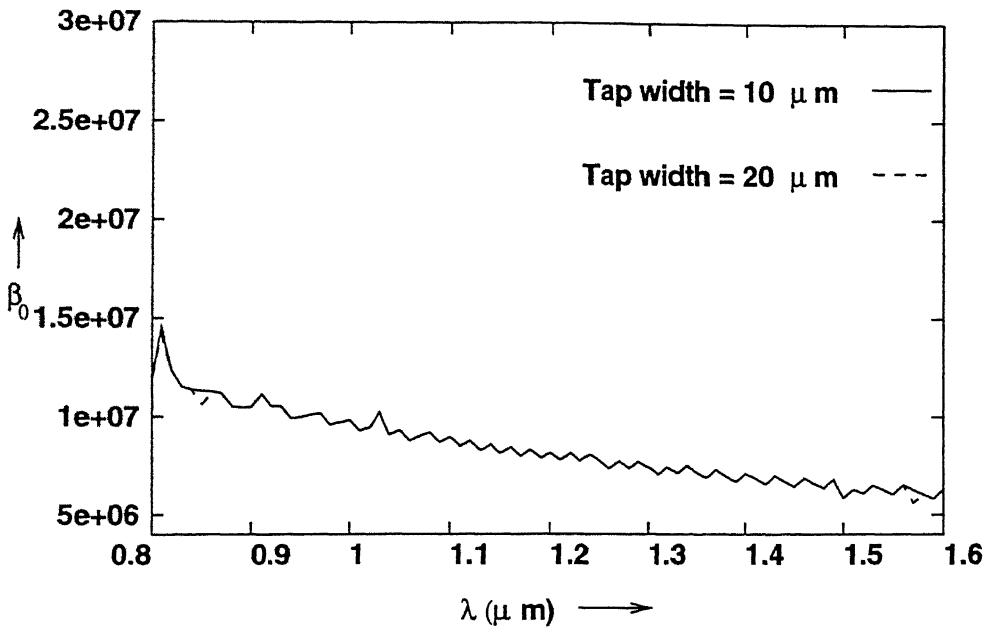

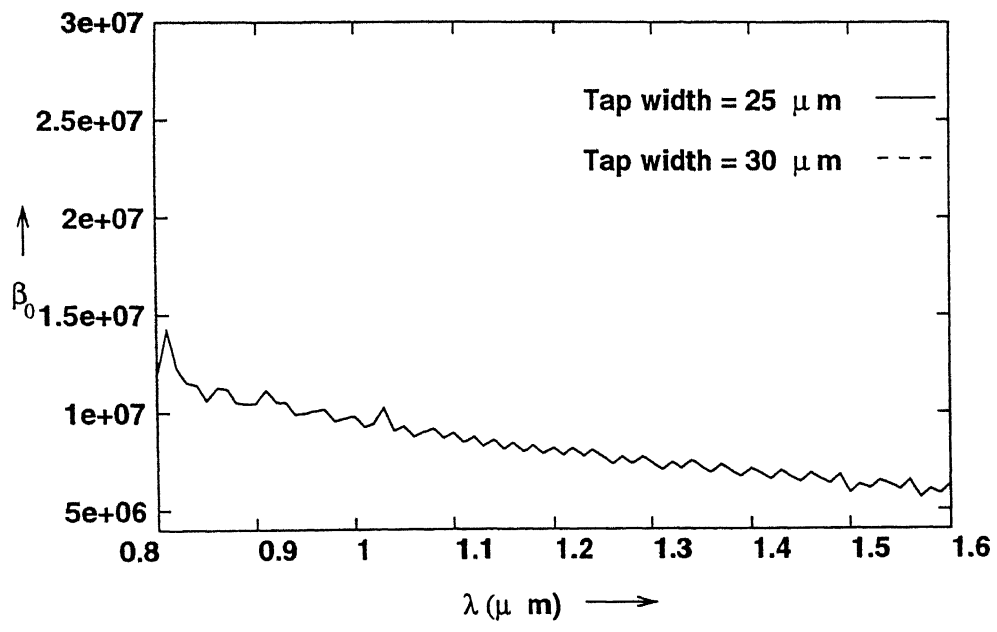

Figure 4.9: Variation of width of taps in rectangular taps

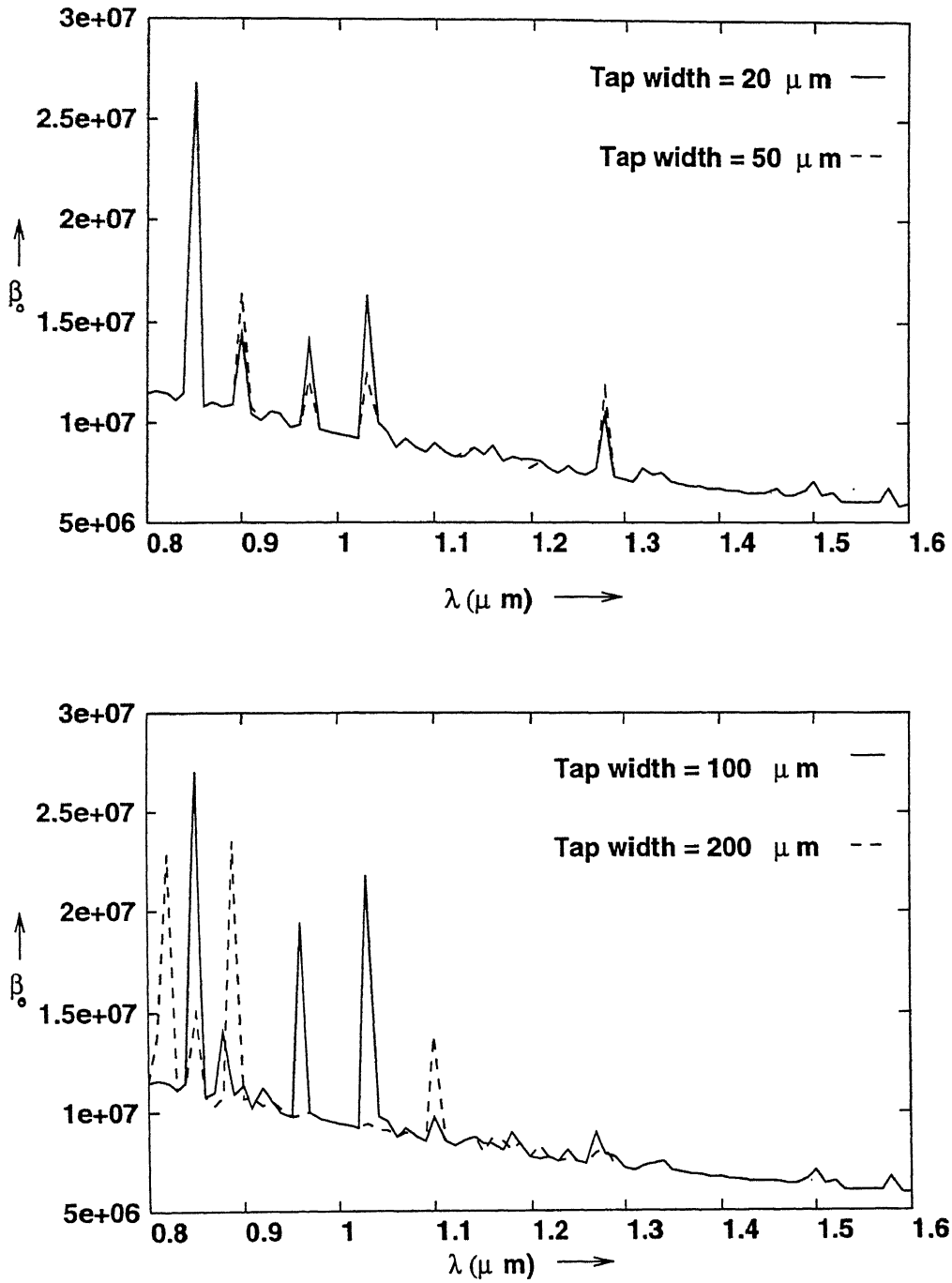

Figure 4.10: Variation of width of taps in triangular taps

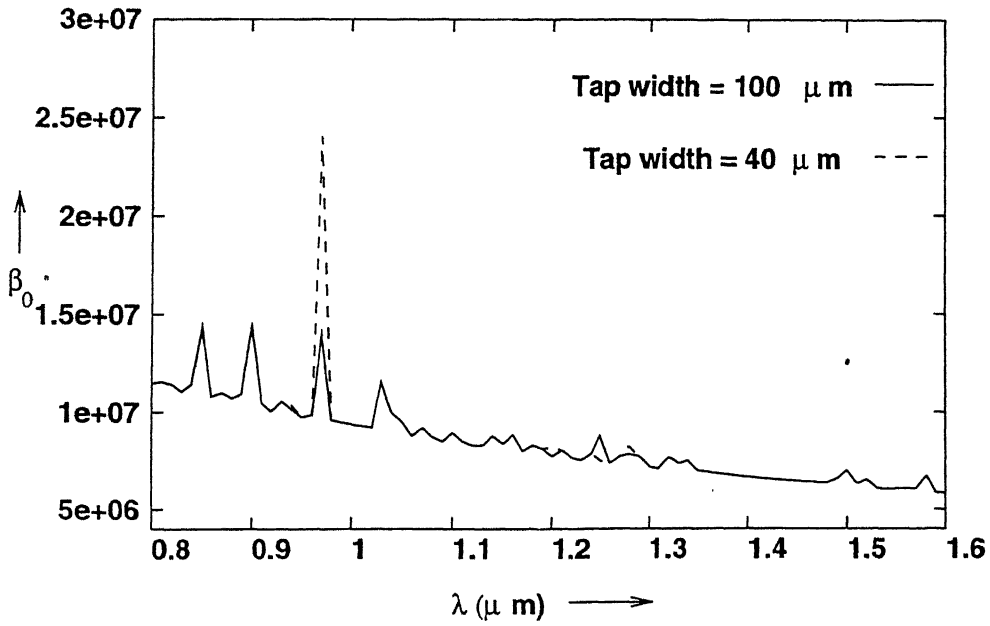

Figure 4.11: Variation of width of taps in gaussian taps

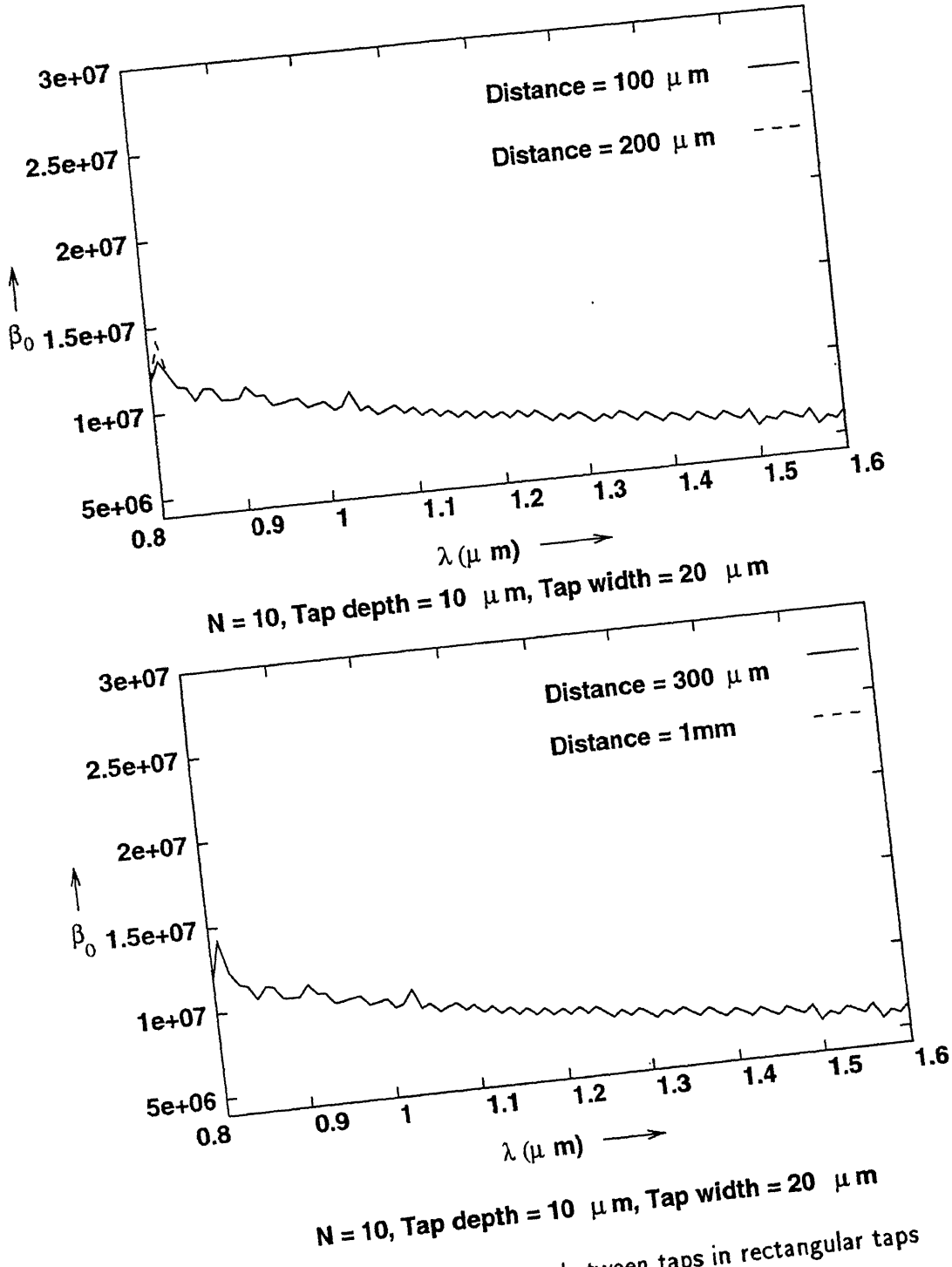

Figure 4.12: Variation of distance between taps in rectangular taps

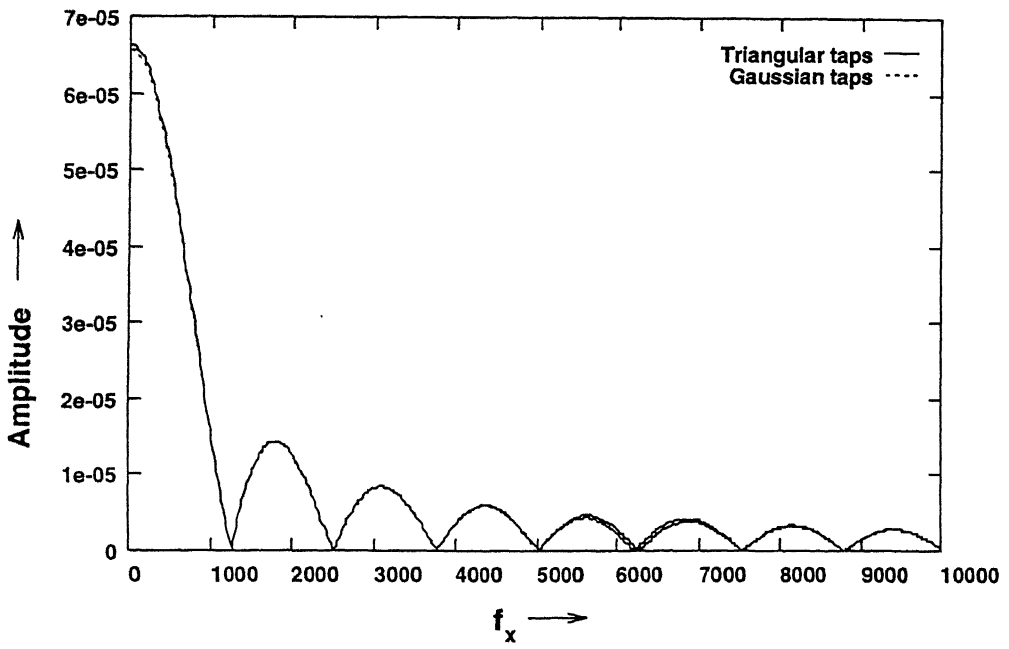

Figure 4.13: Spatial frequency spectrum of Triangular and Gaussian taps

Chapter 5

Conclusions

In this thesis we carried out a numerical simulation of the effect of a series of radiative LACE made taps on the propagation characteristics of optical fibers. We use a spectral/mode-matching method for our analysis. The various parameters that have been looked into are the effect of tap shape, tap depth, tap width and the number of taps on the propagation constant β_0. The following conclusions were obtained from our observations of the results that we obtained.

- The effect of taps is to increase the propagation constant.
- As the number of taps is increased the propagation constant also increases.
- The propagation constant increases with the increase in the tap depth.
- The propagation constant increases with the increase in the width of the tap, however not much increase was observed when compared with the other parameters.
- The use of the package so developed to investigate the propagation characteristics of any dielectric waveguide is also evident since, all the parameters entering as inputs to the program can be varied.
- The results so obtained show a relatively strong dependence of the taps, on the propagation characteristics of the optical fibers, when compared with the other parameters.

5.1 Suggestions for future work

The following are the suggestions for the further work that can be done, to understand more about the behaviour of tapped optical fibers.

- The investigations have been carried out on the rectangular slab waveguide in this thesis, however the method can be extended to the actual optical fiber.
- Further investigations can be carried out on multi-mode fibers and rectangular slabs as well.
- In this thesis we have concentrated on the general solution of the Helmholtz equation, further work can be carried out to obtain the particular solution, so that radiative properties of the taps can also be studied.
- The effect of the material dispersion on the propagation characteristics can be included.
- A similar study can be carried out by filling the taps with various dielectric materials.
- The seemingly strong dependance of the various tap parameters on the propagation characteristics of the optical fiber, can be used in the design of optical fibers with the desired value of propagation constant at a given frequency. This property can then be utilised in design of dispersion flattened and dispersion shifted fibers.

To conclude it can be said that the laser etched fiber optic taps do have a significant effect on the propagation characteristics of the optical fibers. It can be expected that they play a important role in future in optical fiber communication systems, and this work is only a small step in that direction.

Appendix A

Fourier transform

The spatial fourier transform of a function $f(x)$ is given by

$$F(k) = \int_{-\infty}^{\infty} f(x) e^{(-jkx)} dx \tag{A.1}$$

where k is the spatial frequency.

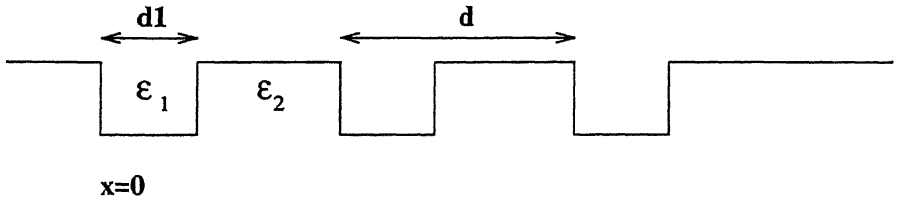

Figure A.1: Profile for Rectangular taps

The fourier transform for the rectangular tapped structure can be derived by viewing the taps as a change in permittivity of the material. ϵ_1 is the permittivity of tap and ϵ_2 the permittivty of the cladding. The taps are assumed to be made from x=0 to x=Nd, where N is the number of taps and d is the distance between taps. If the width of tap is assumed to be equal to d1. The fourier transform for a single tap is then given by

$$F(k) = \int_0^{d1} \epsilon_1 e^{(-jkx)} dx + \int_{d1}^{d} \epsilon_2 e^{(-jkx)} dx \tag{A.2}$$

by integrating, we have

$$F(k) = \frac{1}{jk}[\epsilon_1(1 - e^{(-jkd1)}) + \epsilon_2(e^{(-jkd1)} - e^{(-jkd)})] \tag{A.3}$$

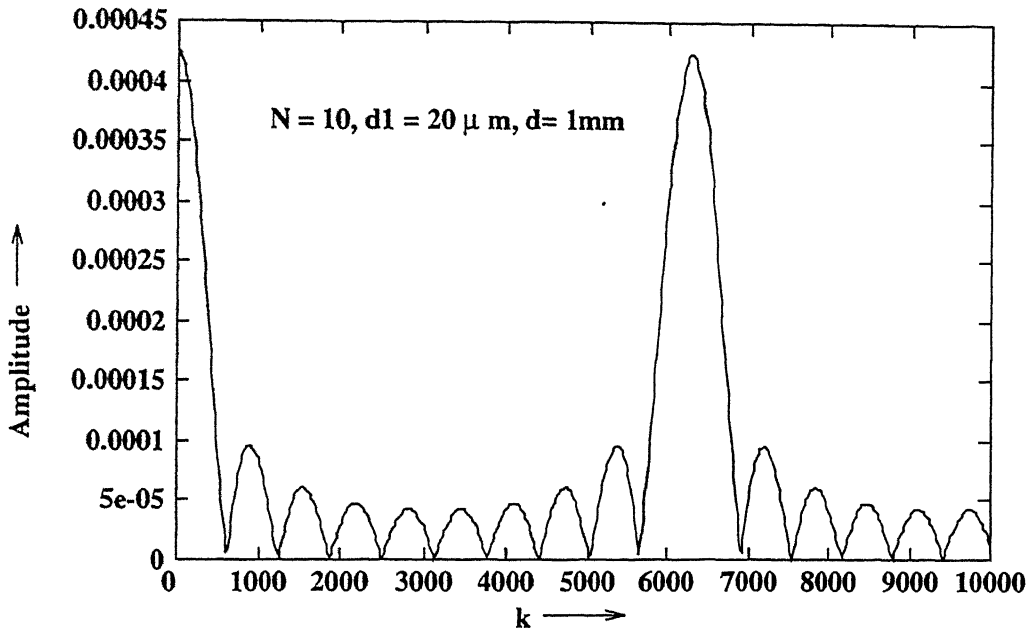

Figure A.2: Fourier transform

The fourier transform for the entire structure is then given

$$G(k) = F(k)[1 + e^{(-jd)} + e^{(-j2d)} + \cdots + e^{(-j(N-1)d)}] \qquad \text{(A.4)}$$

the above equation then reduces to

$$G(k) = F(k)[\frac{1 - e^{(-jNd)}}{1 - e^{(-jd)}}]. \qquad \text{(A.5)}$$

Bibliography

[1] S.T.Peng, T.Tamir, H.L.Bertoni, "Leaky-wave analysis of optical periodic couplers", *Electron.Lett.*, Vol.9, pp. 150-152, 1973.

[2] C.Lee,R.R.Atkins,H.Taylor, "Reflection tapped optical fiber transversal filters", *Electron.Lett.*, Vol.23, No. 11, pp. 596-598, 1987.

[3] M.Kagami, Y.Sakai, H.Okada, T.Ito, "Plastic optical fiber tap", *Opt. Eng.*, Vol. 27, No. 11, 1988.

[4] D.S.Shenk, G.Cohen, "Fiber optic tapping via induced scattering", *J. Lightwave Tech.*, Vol.7, No. 10, pp. 1550, 1989.

[5] S.T.Peng, T.Tamir, H.L.Bertoni, "Theory of periodic dielectric waveguides", *IEEE Trans. Microwave Theory Tech.*, Vol.MTT-23, pp. 123-133, 1975.

[6] Charles Elachi, "Waves in active and passive periodic strucrures", *Proc.IEEE.*, Vol.64, pp. 1666-1698,Dec 1976.

[7] S.T.Peng, T.Tamir, H.L.Bertoni, "Analysis of periodic thin-film structures with rectangular profile", *Opt.Commun.*, Vol.10, pp. 91-94, Jan 1974.

[8] L.R.Lewis, A.Hessel, "Propagation characteristics of periodic arrays of dielectric slabs", *Opt.Commun.*, Vol.10, pp. 91-94, Jan 1974.

[9] A.C.Cangellaris, M.Gribbons, G.Sohos, "A Hybrid Spectral/FDTD Method for the Electromagnetic Analysis of Guided Waves in Periodic Structures ", *IEEE Microwave and Guided Wave Letters*, Vol.3, No. 10, pp. 375-377, Oct 1993.

[10] N.S.Kapany, J.J.Burke, "Optical Waveguides", *Academic Press, Inc., New York*, 1972.

[11] C.Vassallo, "Optical Waveguide Concepts", *ELSEVIER Amsterdam, New York*, 1991.

[12] M.S.Sodha, A.K.Ghatak, "Inhomogeneous Optical Waveguides", *Plenum Press, New York*, 1978.

[13] K.Imen, C.M.Lee, Y.Y.Yang, S.D.Allen, A.Ghosh, "Laser Fabricated Fiber-Optic Taps", *Optics Lett.*, Vol.15, No. 17, pp. 950-952, Sep 1990.

[14] A.K.Ghatak, K.Thyagarajan, "Optical Electronics", *Cambridge Univ. Press*, 1991.

[15] S.Chu, S.K.Chaudhari, "A Finite-Difference Time Domain method for Analysis of Guided-Wave Optical Structures", *J. of Lightwave Technol.*, Vol.7, No. 12, pp. 2033-2038, Dec 1989.

[16] W.Magnus, S.Winkler, "Hill's Equation", *John Wiley & Sons, Inc.*, 1966.

[17] G.Keiser, "Optical Fiber Communications", *McGraw-Hill, Inc.*, 1983.

[18] N.Brillouin, "Wave Propagation in Periodic Structures", *Dover Publications, Inc., New York*, 1956.

[19] The 1994 Newport catlog.